Polymer-Based Composite Materials: Characterizations

2

Jayesh Cherusseri, Sumit Pramanik, L. Sowntharya, Deepak Pandey, Kamal K. Kar, and S. D. Sharma

Contents

J. Cherusseri • L. Sowntharya • D. Pandey
Advanced Nanoengineering Materials Laboratory, Materials Science Programme, Indian Institute of Technology Kanpur, Kanpur, Uttar Pradesh, India
e-mail: jayeshpuli@gmail.com; sowsindhu@gmail.com; dpandey@oceaneering.com

S. Pramanik
Advanced Nanoengineering Materials Laboratory, Materials Science Programme, Indian Institute of Technology Kanpur, Kanpur, Uttar Pradesh, India

Department of Biomedical Engineering, Faculty of Engineering, University of Malaya, Kuala Lumpur, Malaysia
e-mail: prsumit@gmail.com

K.K. Kar (✉)
Advanced Nanoengineering Materials Laboratory, Materials Science Programme, Indian Institute of Technology Kanpur, Kanpur, Uttar Pradesh, India

Advanced Nanoengineering Materials Laboratory, Department of Mechanical Engineering, Indian Institute of Technology Kanpur, Kanpur, Uttar Pradesh, India
e-mail: kamalkk@iitk.ac.in

S.D. Sharma
Advanced Nanoengineering Materials Laboratory, Materials Science Programme, Indian Institute of Technology Kanpur, Kanpur, Uttar Pradesh, India

Department of Mechanical Engineering, Rewa Engineering College, Rewa, India
e-mail: sds1970@gmail.com

K.K. Kar (ed.), *Composite Materials*,
DOI 10.1007/978-3-662-49514-8_2

Abstract

Various types of composite materials are becoming an inevitable part of our day-to-day life since these are used for a variety of applications. A better understanding on the various properties of the composites is very helpful in their targeted applications, and hence characterizing the composite materials by different techniques play a major role in the development of long-life, high-quality composite products. The polymer-based composite materials provide large amount of flexibility and lightweight to the final product. The selection of various reinforcements and polymer matrices is very critical in designing a desired product. In this chapter, various techniques used for characterizing the polymer-based composite materials in order to examine their mechanical, thermal, electrical, magnetic, piezoelectric, tribological, rheological, and biological properties are discussed.

Keywords

Creep • Fatigue • Flexural strength • Glass transition temperature • Piezoelectric • Polymer composite • Scanning electron microscopy • Stiffness • Stress relaxation • Voids

Introduction

Composite materials have been in use for thousands of years. For example, mud bricks, which are composed of mud (matrix) and straw (reinforcing fiber), can resist both tensile and compressive loads, thus resulting in an excellent building material. It is a combination of at least two materials, one being a binding material (or matrix) and the other one is a reinforcing material. The matrix holds the reinforcing materials together. However, many composite products are made with more than two raw materials, but those materials are not miscible together and have different nature. Composites exist in nature and can be made by humans also. A good example for a natural composite is wood. It consists of long fibers of cellulose bound together by a much weaker substance called lignin. There are several kinds of man-made

composites like structural beam, which is an inhomogeneous mixture of cement (matrix), stone (reinforcing particle), and steel rod (reinforcing fiber). The selection of materials for the matrix and reinforcement, the form of reinforcement, and the manufacturing process are very critical for obtaining a composite product with desired properties. The matrix material can be a metal, ceramic, glass, polymer, or organic material in solid (plate or powder) or semisolid forms. The reinforcing material can be a metal, ceramic, glass, textile, polymer, or organic material in the form of lamina, fiber (short and long), particle, whisker, etc. The main advantage of composite material is their high strength and stiffness combined with lightweight feature. The composites have major applications in the advanced fields such as structure, thermal engine and blade, automobile, aerospace, rocket, missile, satellite, military, biomedical, electronics, packaging, etc. The characterization of a composite is one of the essential tasks for developing the desired composite products for particular applications. The major characterization studies used for composites for the evaluation of performance in the targeted areas are mechanical, thermal, electrical, magnetic, piezoelectric, tribological, rheological, and biological.

Volume Fraction

In a composite material, the parameter "volume fraction" plays a major role in characterizing its various properties such as mechanical, thermal, electrical, etc. The evaluation of this parameter is of great importance for material scientists. For example, in a fiber-reinforced composite, the fiber volume fraction significantly determines its properties. A composite can't be prepared with 100 % of fibers. There is a maximum limit of fiber content in a composite structure. And this maximum volume fraction is able to achieve only when the unidirectional fibers are hexagonally close packed. For a composite material, let the total volume be "V" and masses of its constituent materials be M_1, M_2, M_3, etc. Then the composite density (ρ_{com}) can be expressed (Eq. 2.1) as

$$\rho_{com} = \frac{M_1}{V} + \frac{M_2}{V} + \frac{M_3}{V} + \ldots \tag{2.1}$$

In terms of the densities and volumes of the constituents, Eq. 2.1 can be written as Eq. 2.2 based on the rule of mixtures.

$$\rho_{com} = \frac{V_1 \rho_1}{V} + \frac{V_2 \rho_2}{V} + \frac{V_3 \rho_3}{V} + \ldots \tag{2.2}$$

where V_i and ρ_i are the volume fractions and densities of the i^{th} phase, respectively.

The fiber volume fraction (V_f) can be written in terms of fiber weight fraction (W_f) [1] as

$$V_f = \frac{W_f \rho_m}{W_f \rho_m + W_m \rho_f} \tag{2.3}$$

where ρ_m, ρ_f, W_f, and W_m are the density of the matrix, the density of the fiber, the weight fraction of the fiber, and the weight fraction of the matrix, respectively. Correspondingly, the fiber weight fraction (W_f) can be expressed in terms of fiber volume fraction (V_f) [1] as

$$W_f = \frac{V_f \rho_f}{V_f \rho_f + V_m \rho_m} \tag{2.4}$$

The fiber volume fraction determines the strength of the composites. Ravi et al. have studied the effect of fiber volume percent on the dynamic damage behavior of woven glass fiber-reinforced polymer (FRP) composites [2]. Delamination is the major damage noticed for specimens with higher fiber volume percent, while the matrix cracking and interface debonding occurs for materials with low fiber volume percent. Fiber volume percent in combination with fiber distribution is the main parameter affecting the interlaminar fracture toughness (ILFT) [3]. It has a significant influence on the longitudinal tensile and compressive strengths and the in-plane shear strength of FRPs. The strength parameters vary in direct proportion to the fiber volume percent up to 50 % [4]. The fiber volume percent of a composite are determined by chemical matrix digestion method as described in ASTM D3171 [5], the burn test as described in ASTM standard D2584 [6], or by photomicrographic techniques. For glass fiber composites, burn test is used because the glass shows good oxidation resistance (500–600 °C), which is much more than the complete burning of matrix.

Voids

Voids form at the interface of composite structures. These are generally formed as gas bubbles trapped inside the cured composite materials. The main sources of voids include the material constituents and the synthesis processes. The presence of voids in a composite structure is found to affect its structural and mechanical properties. It has been predicted that the interlayer and intra-layer reactions caused by the stress and chemically driven diffusion are responsible for the usual void behavior in composites. Voids present in the composite material can be evaluated by matrix digestion and matrix burn-off techniques [1].

The volume fraction of void (V_{void}) can be calculated if the composite density and the density of the matrix and fibers are known. The equation for determining the volume fraction of void is given by Eq. 2.5 [1] as

$$V_{void} = 1 - \rho_{com}^{exp}\left(\frac{W_m}{\rho_m} + \frac{W_f}{\rho_f}\right) \tag{2.5}$$

where ρ_{com}^{exp} is the experimentally determined composite density. Void is undesirable and has adverse effect on the mechanical properties of composites. Wu et al. have developed an analytical model to estimate the elastic properties of polymer composites with voids of various sizes and locations [7]. These voids have significant influence on the interlaminar shear strength (ILSS) of the composite materials

[8]. Bowles and Frimpong have studied the influence of voids on the ILSS of graphite fiber-reinforced PMR-15 composites [9]. As the void content increases, an increase in scatter in the strength data is observed. The role of voids in the initiation and propagation of cracks in composites reinforced with unidirectional carbon fiber (CF) has been investigated by Chambers et al. [10]. Void area greater than 0.03 mm^2 results in deterioration of mechanical properties. Voids assist in the propagation of crack in the resin-rich interply regions. An increased void content increases composite's susceptibility to water penetration and weathering. The procedure of measuring the voids in composites, required for the calculation of density, is given in ASTM D 1505 [11] and ASTM D 3800 [12].

Surface Roughness

Surface roughness is an important parameter for ascertaining the surface quality and aesthetic value. The average surface roughness (Ra value) is one of the most frequently used parameters for surface roughness, which describes the height of irregularities and gives an indirect indication of the sharpness and depth of surface notches [13]. It is an absolute average roughness over one sampling length [14]. Researchers have used this Ra value for studying the impacts of various process parameters on the surface quality of FRP composites. Davim and Reis have analyzed the effects of machining parameters on the surface quality of plastics reinforced with CFs [15].

Surface Topography

Scanning electron microscope (SEM) is also used for studying the topography of solids [16]. In the field of FRPs, it is used to reveal the actual distribution of fibers and matrix in the composite. It is also used for the analysis of fractured surfaces [17] and helps to examine the crack propagation in fibrous composite materials in order to gain an insight about composite strength, the adhesion between the phases, and the mode of failure [18]. It serves as an effective means to confirm the uniformity of fiber distribution across the cross section and presence of internal flaws (like voids, broken fibers, foreign inclusions, etc.) at microscopic level, which explain the physical and mechanical behavior of composites and the discrepancies associated with their properties.

Mechanical

Measurement of mechanical properties of composites involves testing on the suitably designed specimens. The interpretation of material response over the entire range of loads is necessary, if the advanced design procedures are to be used for the efficient material utilization. The macromechanical properties of composites may be computed through micromechanical analysis, and the design of composite materials may be started with constituent material properties. However, the validity of

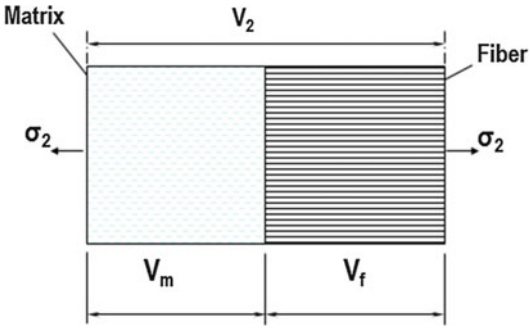

Fig. 2.1 Schematic of slab model showing transverse stiffness of a unidirectional composite

micromechanical analysis is to be checked through experiments. Another purpose of mechanical characterization is to check the adequacy of new fabrication procedure and to assure the material uniformity. The mechanical properties of composites include (i) strain and yield strength in tension, compression, shear, and torsion, (ii) ILSS between the matrix and fiber, (iii) flexural fatigue strength, (iv) impact strength, (v) stress relaxation, and (vi) creep.

Strength

A high strength-to-weight ratio is required for a composite in its applications. Hence, it is very important to determine its strength. Thus, characterizing the strength of a composite is very critical before its application. This section briefly discusses about the various mechanical characterization tools used for finding out the strength of the composite materials.

Tensile Strength The ASTM standard D-3552-96 defines the test method for determining the tensile properties of a fiber-reinforced metal matrix composite (MMC). However, the tensile properties of advanced composite materials and polymer matrix composites can be tested by ASTM standard D-3039, and the tensile properties of MMCs can be characterized by ASTM standard D-3518 specimen. Strength characteristics of composite materials generally follow the mixture rules. These are mathematical expressions giving the property of the composite in terms of the quantity and arrangement of its constituting materials. Let us assume a part of the unidirectional composite material having unit dimensions with the fibers having volume fraction, V_f. Then, the volume fraction of the matrix, V_m (Eq. 2.6), is given [19] as

$$V_m = 1 - V_f \tag{2.6}$$

The slab model is shown in Fig. 2.1.

If a stress σ_1 is applied in a direction of the fiber orientation, then both the fiber and matrix act parallel to resist the load. In this case, strain in both fiber (ε_f) and

matrix (ε_m) must be the same (let it be ε_1) in fiber direction and can be written (Eq. 2.7) as

$$\varepsilon_f = \varepsilon_m = \varepsilon_1 \tag{2.7}$$

It is clear that the load on the composite must be equal to the sum of the total load of the fiber phase and the matrix phase. Load on each phase is the phase area times the stress in each phase, but phase area is numerically equal to its own volume fraction. Hence, the composite strength (σ_{com}, Eq. 2.8) can be written [19] as

$$\sigma_{com} = \sigma_f V_f + \sigma_m V_m \tag{2.8}$$

where, σ_f, σ_m, V_f, and V_m are the total stress on the fiber phase, the total stress on the matrix phase, the volume fraction of the fiber phase, and the volume fraction of the matrix phase, respectively.

Consider the ultimate strained condition of the fibers in the unidirectional composite at which the fiber begins to break. The breaking strength of the composite (σ_b) can be written from the rule of mixtures [19] as

$$\sigma_b = \sigma_{fb} V_f + \sigma_{mb}(1 - V_f) \tag{2.9}$$

where σ_{fb} and σ_{mb} are the breaking strength of the fiber and the breaking strength of the matrix, respectively. At the breaking strain of the fiber, the load carried by the fiber becomes zero, which results in transferring the entire load to the matrix. The breaking strength of the composite is now reduced according to the fiber fraction as

$$\sigma_b = \sigma_{mb}(1 - V_f) \tag{2.10}$$

The maximum of these two strengths gives the breaking strength of the whole composite. For a certain range of fiber fraction in the composite, the strength actually reduces on the addition of fibers. These relations are presented in Fig. 2.2.

The tensile properties of the composites can also be determined by bending a sandwich beam specimen containing a thin layer of composite material, which is bonded to the top and bottom of a thick substrate such as an Al honeycomb [20, 21]. This method can also be used for determining off-axis properties and transverse properties as reported by Lantz [21]. Richards et al. have showed that the satisfactory results can be achieved for 45^0 specimens having a value of 12 for the ratio of the specimen length between the grips to its width [22]. Pagano and Halpin have found that a uniform state of strain and stress exists at the center of an off-axis tensile coupon if the length-to-width ratio is sufficiently large [23]. A standard test method to determine the tensile properties of polymer matrix composite materials has been described in ASTM D3039 [24].

The strength and toughness are the properties that are strongly enhanced by the addition of nanoparticles in the matrix. This is not only observed in the polymer matrix composites but also in other composites. For example, certain nanoconstituents like silicon carbide (SiC), silicon nitride (Si_3N_4), etc. are added

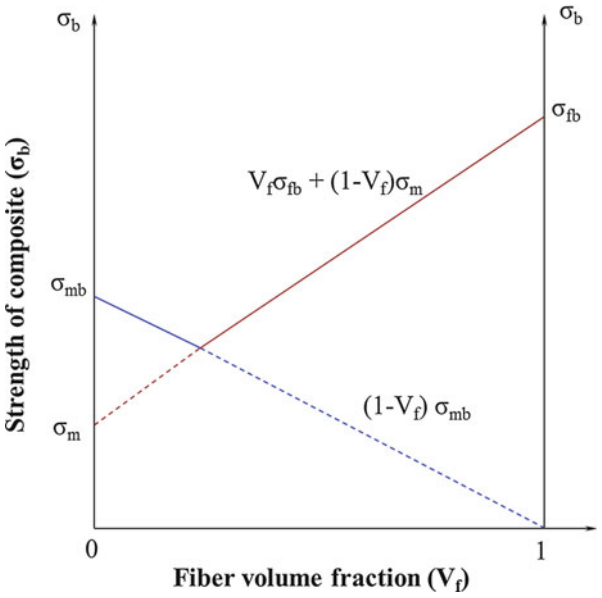

Fig. 2.2 Schematic showing the strength of a unidirectional composite in fiber direction

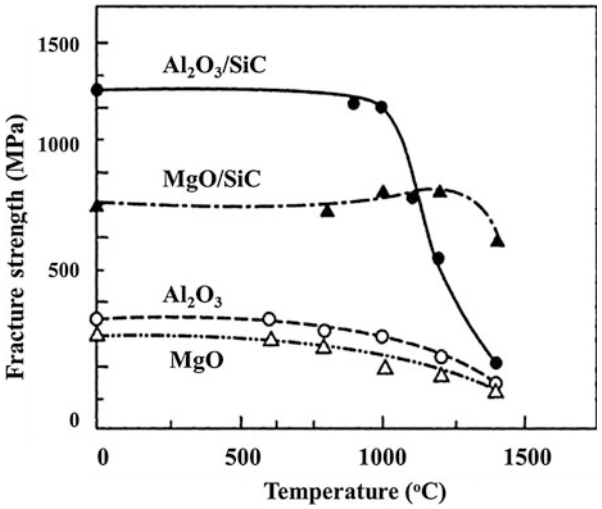

Fig. 2.3 Temperature dependence fracture strength for ceramic oxides and ceramic nanocomposites [25]

into the non-polymer matrix like alumina to form Al_2O_3/SiC, Al_2O_3/Si_3N_4, MgO/SiC, and SiN_4/SiC nanocomposites. The strength of alumina is almost three times augmented with the help of the dispersion of 5 vol.% SiC nanoparticles in the alumina matrix. It has been observed that the annealing also helps to improve the fracture strength by the development of sub-grain boundaries. For example, in the case of MgO/SiC nanocomposite, the annealing enhances its fracture strength over a wide temperature range [25]. A significant improvement of high-temperature

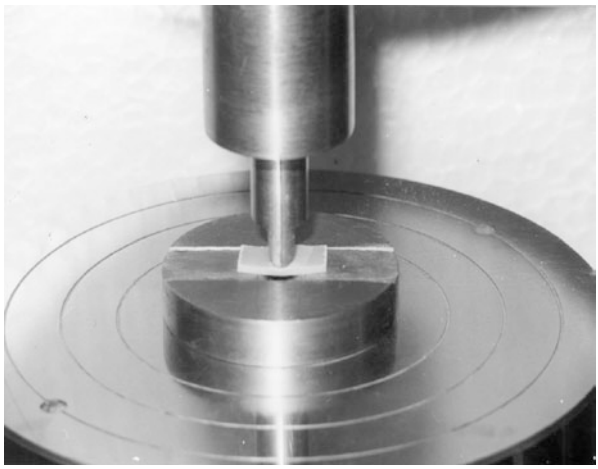

Fig. 2.4 Experimental setup to measure the interlaminar shear strength

strengths for Al_2O_3/SiC and MgO/SiC nanocomposites with respect to Al_2O_3 and MgO matrices is shown in Fig. 2.3.

Flexural Strength In a bend test of a specimen, bending strength of the outermost fiber at the instant of failure is defined as flexural strength. The nominal flexural strength (σ_N, Eq. 2.11) can be written [26] as:

$$\sigma_N = f_r^o \left(1 - \frac{D_b}{D}\right)^{-1} \tag{2.11}$$

where f_r^o is the average tensile strength of the boundary layer and is given by

$$f_r^o = \frac{M_o(D - D_B)}{2I} \tag{2.12}$$

where M_o, D, D_b, and I are the bending moment, the beam depth, the half value of boundary layer thickness, and the moment of inertia of cross section, respectively. The expression for moment of inertia (I) can be written as

$$I = \frac{D^3}{12} \tag{2.13}$$

Plastics have higher flexural strength as compared to their straight tensile. The breaking force required for a specimen of specified width and thickness is known as "modulus of rupture."

Interlaminar Shear Strength Evaluation of ILSS can be done by a similar test procedure adopted for the flexural strength. The experimental setup is shown in

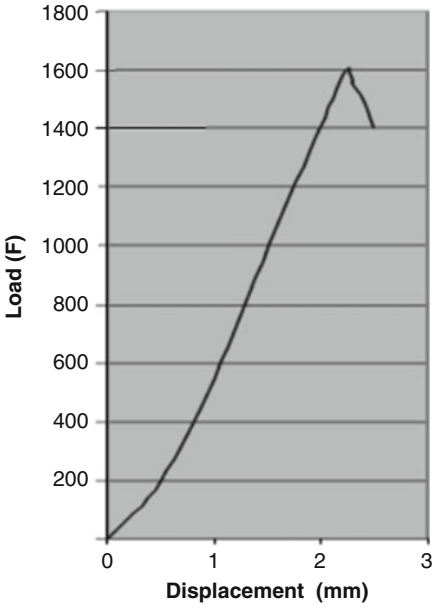

Fig. 2.5 Load versus displacement curve during a test for determining ILSS

Fig. 2.4. The composite specimen dimensions and geometry are recommended in ASTM D-3039-79 and ASTM D-3410 in tension and compression mode, respectively, and ASTM D-695 for advanced composite materials in compression mode. The ILSS (τ, Eq. 2.14) can be expressed [27] as follows:

$$\tau = \frac{3F}{4bd} \tag{2.14}$$

where F, b, and d are the load at the moment of break, the width of the specimen, and the thickness of the specimen, respectively. A representative curve of load versus displacement for a specimen under testing is shown in Fig. 2.5.

Hsu and Herakovich have examined the problem by separating each layer into an outer and an inner region [28]. The inner region is analyzed using classical laminate theory, while the region near the free edge is analyzed by employing the perturbation technique and concluded that their analysis renders better results than the finite difference solution by Pipes and Pagano [29]. Wang and Dickson have developed a method to calculate the interlaminar stresses in symmetric composite laminates [30]. They have used the extended Galerkin method with the interlaminar stresses, and the displacements are represented by complete sets of Legendre polynomials. This method provides systematic steps for direct computation of interlaminar stresses. A substantial study has been reported on the ILSS of composite materials at room temperature. ILSS depends on the resin formulation [31–35]. A group of researchers has altered the resin to improve the ILSS of composites [36–41]. Another group of researchers has altered the fiber surface using elastomer [42], silane [43, 44], styrene

[45], styrene–isoprene [46], polybutadiene [47], methacryloxypropyltrimethoxysilane [46], methacryloxypropyltrimethoxysilane-modified polybutadiene [46], and oxidation to improve the ILSS of composites made of epoxy [42, 45], phenolic [43], nylon 6 [44], and vinyl ester [47]. The dependence of ILSS on fiber orientations of the neighboring plies around the interfaces has been studied extensively by Zhang et al. [48], Okada and Nishijima [49], Vishwanath et al. [50], and Costa et al. [51]. Ray has studied the ILSS of epoxy composites having glass fiber loading of 55, 60 and 65 % by weight [52, 53]. A rapid decrease in ILSS with increasing void content in FRP composites is reported by Costa et al. [51] and Mouritz [54]. Ray [52, 53] has studied the impact of strain on ILSS.

Impact Strength The impact strength of a composite is a very important design parameter in most of the applications, e.g., aeronautics (bird impact on the engine), and personal vehicle armors. An analytical solution of the transversal impact on a yarn has been developed by Smith in 1958. In a yarn point impact for an elastic material, the transverse and longitudinal waves propagate with respective velocity (U, Eq. 2.15) written [55] as

$$U = C\left[\sqrt{\varepsilon(1+\varepsilon)} - \varepsilon\right] \tag{2.15}$$

where C and ε are the strain–wave velocity and strain of the yarn, respectively. The strain–wave velocity (C) can be determined from Eq. 2.16 [55]:

$$C = \frac{2L(1+3\varepsilon) + d_2}{t_2(1+2\varepsilon)} \tag{2.16}$$

where L, d_2 and t_2 are the strain–wave front traveling distance after reflection at the clamp, the distance traveled by the transverse wave after reflection, and the transverse wave overtaking time after reflection.

Chocron-Benloulo et al. have shown the trend of residual velocity with striking velocity analytically, for 8 ply Kevlar 29 panel shot by a 64 grain (4.147 g) fragment simulating projectile, where the striking velocity was 300–1500 m/s [56]. This analytical model is shown in Fig. 2.6.

An experiment has been conducted on a mechanically needle-punched nonwoven fabric, which is made of natural fiber [57]. Polypropylene is used as a polymer binder fiber, and the natural fibers used are flax, hemp, and kenaf. The blending ratios of natural/polymeric fiber are varied from 50/50 to 70/30. The fiber or polypropylene mats are used as a reference material. The prepregs weight ranges from 1600 to 2400 g/m^2. The objective of this experiment is to measure the dynamic stress using a reflection polariscope with single-flash technique. The impact test apparatus consists of a loading apparatus and a photoelastic element setup as illustrated in Fig. 2.7. In this process, pressurized air is used to accelerate the steel projectile and an anvil is used to transmit the impulse. It uses a piezoelectric force sensor and avoids damaging the composite at the contact point. The boundary conditions are different for

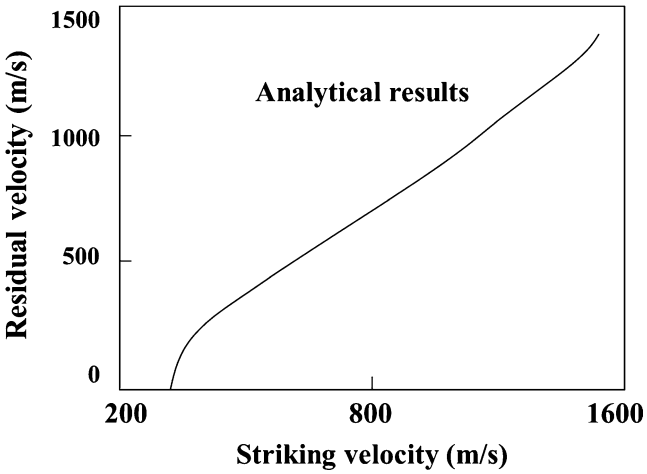

Fig. 2.6 Analytical model of residual velocity versus striking velocity for 8 ply Kevlar 29 panel [56]

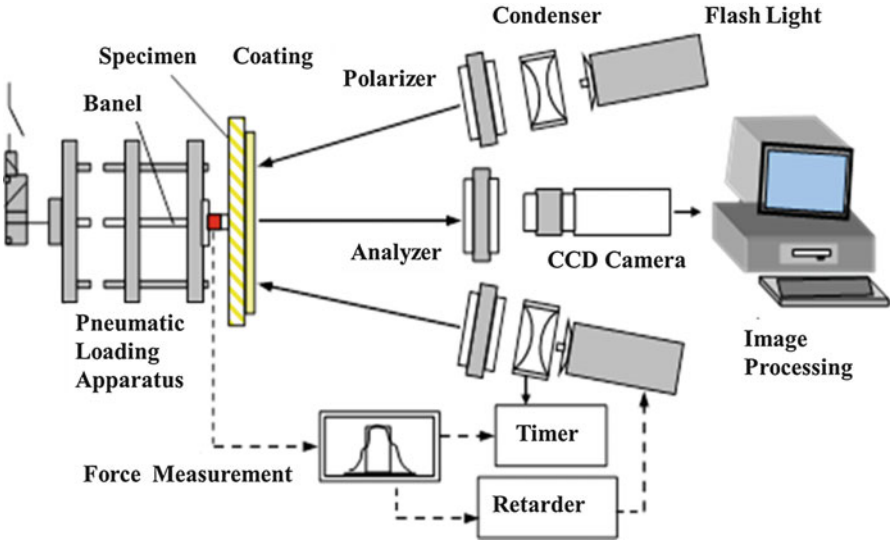

Fig. 2.7 Schematic of impact testing device [57]

various specimens like disk, beams, or plates, which are in the loading apparatus. Now, the wave propagation can be very easily detected in its early stages (provided that the reflection should occur at the point of interest of the specimen). It is possible to investigate the effect of superposition and reflection of propagating waves at different profile and/or boundary conditions. It also helps in understanding the fracture nature of FRP composites after the impact loading. The applications of the test are (i) locating the artificial cracks by analyzing impact strains in the specimen, (ii) determining the viscoelastic properties of composites and photoelastic coating

material due to high strain rates, (iii) analyzing the strain–wave propagation in FRP composite disks, (iv) having the ability to trace stress concentration in the impact-loaded orthotropic composites, etc.

Another procedure to determine the impact toughness is notched Izod test. The hammer has been dropped from a height of 0.6 m with a velocity of 3.4 m/s. This test is used to determine the impact behavior of composites with end-shaped fibers. The impact toughness depends on the various parameters like behavior of the matrix, fiber end, and fiber length.

Notch Strength Geometry effects, locally concentrated damages, and notches influence the local stress concentration. The presence of notch is the main reason for the failure of composite materials. This is due to the square planar array of broken fibers. The extents of fiber pullout and the stress concentration around the notch lead to failure. The extent of fiber pullout mainly depends on the Weibull modulus. Normalized notch strength (σ, Eq. 2.17) can be written as follows [58]:

$$\sigma = \frac{\mu*}{c_i} + \sigma_p \tag{2.17}$$

where μ^*, c_i, and σ_p are the strength of the critical link at the notch, the notch size, and the normalized pullout stress, respectively. The expression for normalized pullout stress (σ_p) is given by Eq. 2.18 [58].

$$\sigma_p = \left(\frac{1}{m+1}\right)^{\frac{m}{m+1}} \Gamma\left(\frac{m+2}{m+1}\right) \tag{2.18}$$

where m is the Weibull modulus.

The notch strength of composite (σ_f^*) is given by Eq. 2.19 [58].

$$\sigma_f^* = \left[\frac{(c_{i_n} - 1)(m+1)}{n_{i_n}\left(c_{i_n}^{m+1} - 1\right)}\right]^{\frac{1}{m+1}} \tag{2.19}$$

where i_n and n_i are the initial notch size and the number of nearest neighbors, respectively.

The normalized notch strength predicted by an analytical local load-sharing model and by the Batdorf-type model is compared for better understanding. The normalized fiber bundle notch strength (σ_f^*/σ_c) versus initial notch size (i_n) for fiber Weibull moduli (m) of 5 and 10 predicted by the above models are shown in Fig. 2.8. The notch strength predicted by both the models are nearly parallel for $m = 10$, but there is a huge difference in the notch strength obtained by two methods for $m = 5$. According to the Batdorf model, the fibers with $m = 5$ are weaker than $m = 10$, which is in contradiction to the local load-sharing analytical model.

Fracture Toughness Fracture toughness is the energy absorbed by the composite during loading or impact in order to propagate a crack up to the failure. Actual

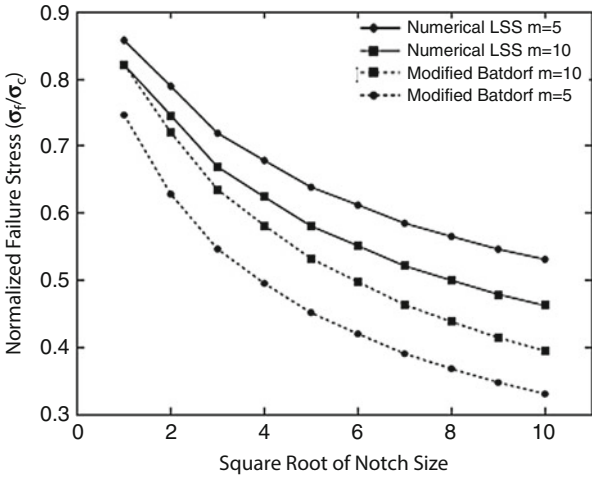

Fig. 2.8 Graph showing notch strength of Ti MMCs [58]

fracture toughness is predicted by a single pullout fiber testing. Fiber properties such as fiber end shape, fiber length, friction at interface, and matrix properties have an influence on the fracture and impact toughness. ASTM D-5528:01 defines the standard test method to determine the mode-I interlaminar fracture toughness of unidirectional FRP matrix composite. However, for the mixed mode-I and mode-II, it is based on the standard number ASTM D-6671/D 6671 M-04e1. Estimation of the fracture load of notched plates is a tedious job but it has been established more or less. The influence of parameters like the notch geometry, notch root radius, notch angle, notch depth, and relative width and thickness of the specimen have been extensively studied. Dash et al. have studied how the critical stress intensity factor K_C is affected by the crack size and environmental effects on fracture toughness [59]. These new experimental procedures are more reliable and have been used for studying the fracture toughness. The total fracture toughness (R_t) is given by Eqs. 2.20, 2.21, and 2.22 [59, 60]:

$$R_t = R_r + R_{po} + R_s \tag{2.20}$$

$$\approx \frac{V_f \sigma_f^*}{\tau_f}\left[\frac{\sigma_f^*.d}{6}\left(\frac{1}{4}+\frac{\sigma_f^*}{E_f}\right)+\frac{R_m}{2}\right]+\left(1-V_f\right)R_m \tag{2.21}$$

$$R_s = V_f R_f + \left(1-V_f\right)R_m + V_f\frac{l_d}{d}R_i \approx V_f\left(\frac{l_d}{d}-1\right)R_m \tag{2.22}$$

where R_r, R_{po}, R_s, R_f, R_m, R_i, d, τ_f, l_d, V_f, and E_f are the toughness due to stress redistribution, toughness due to the fiber pullout, toughness due to a creation of new surface in the fiber, matrix and interface, toughness at the fiber, toughness at the matrix, toughness at the interface, fiber diameter, frictional shear stress, de-bond length, volume fraction of the fiber, and Young's modulus of the fiber, respectively.

For most of the fiber composites with thermoset matrices, particularly with CFs, fiber pullout is the primary source of fracture toughness and is represented by Eq. 2.23 [60].

$$R_{po} = \frac{2V_f \tau_f l_{po}^2}{d} \tag{2.23}$$

where l_{po} = pullout distance. When the critical transfer length (l_c) is more than the fiber length (l), all the fibers are pulled out assuming l_{po} varies from 0 to 0.5 within the mean value of 0.25; the R_{po} is given by Eq. 2.24 [60].

$$R_{po} = \frac{V_f \tau_f l^2}{6d} l \leq l_c \tag{2.24}$$

R_{po} is maximum for $l = l_c$.

For the composite having fiber length (l) greater than the critical fiber length (l_c), the fraction of fiber can be pulled out up to $\frac{l_c}{l}$ and the l_{po} varies from 0 to 0.5.

Therefore, R_{po} is written by Eq. 2.25 [60].

$$R_{po} = \frac{V_f \tau_f l^3}{6d\, l} l > l_c \tag{2.25}$$

Recently, Dash et al. have used an epoxy resin (Araldite–LY5052 and a hardener–HY5052) reinforced by a plain-woven carbon fabric (INDCARF–30 of 3 K-filament counts: a product of IPCL) [59]. A specimen fabricated of CF-reinforced composite with ASTM standard D-3039 dimensions is shown in Fig. 2.9. A thick diamond-edged wheel with thickness 0.03 mm has been used to cut a sharp notch of varying sizes in different specimens.

For a fracture toughness test, a specimen with single-edge sharp notch is used. This specimen is then subjected to a tensile loading on a servo-hydraulic tensile testing machine. It has been clamped initially by using pin-loaded grips. The specimen experiences a monotonic uniaxial tension at a certain displacement rate. Ample precaution has to be taken to maintain a uniform temperature around the test jig. Rate of crack displacement is closely monitored, and the critical load is calculated at the complete fracture load. The fracture equation is given by Eq. 2.26 [61].

$$K_c = \alpha \sigma_{nc} \sqrt{\pi a} \tag{2.26}$$

where K_C, α, σ_{nc}, and a are the notch toughness, the boundary modification factor, the critical nominal stress, and the crack length, respectively.

The delamination results in complete fracture and also reduction in stiffness, which is a very important parameter for designers. The current challenge is to increase the lifetime and load-bearing capacity of the composites by controlling the delamination behavior. The crack plane due to delamination in composites is well defined, and the elasticity of the material is retained in the vicinity of the crack tip except in the very thin layer of interface. Hence, examining the energy release rate assists in analyzing the crack formed. Wilkins et al. have found the critical strain

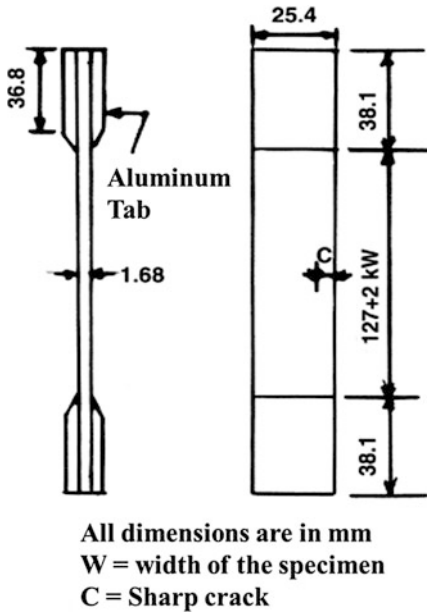

Fig. 2.9 A specimen with ASTM standard D-3039 [59]

energy release rate for mode-I and mode-II delamination [62]. Han and Koutsky have found the interlaminar fracture energy of polyester composites reinforced with glass using width-tapered double-cantilever beam (WTDCB) specimens [63]. A nonlinear theory for the energy release rate using double-cantilever beam (DCB) has been developed by Devitt et al. [64]. Mall et al. have used the DCB specimen to investigate the effect of loading rate on ILFT [65]. A substantial study of ILFT has been reported at room temperature on composite materials comprising glass fiber and polyester resin [66–73]. The ILFT of composite is influenced by the sizing agent [66, 67], materials used as matrix [68, 69], loading of particles [70], geometry of the fabric [71], fiber volume percent [74], fiber orientation of the fiber [72, 75], processing pressure [76], aging condition [68], humidity [69], and temperature [77]. It is clear from the literatures that for structural application of composite materials, ILFT is an important material property.

Modulus or Stiffness

The reinforcements such as fibers in a matrix material may have random or preferred orientations. If the fibers are aligned in the same direction, then they suffer with high stress. Hence, random orientation of material (known as anisotropic, which means that it is having different properties in different directions) is preferred. The most important factor of controlling the anisotropy is the optimization of properties for

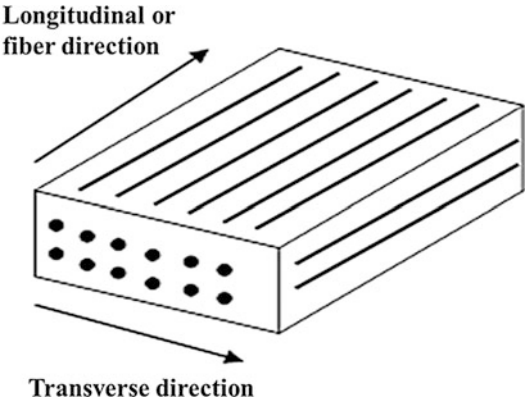

Fig. 2.10 Longitudinal and transverse direction of fiber-reinforced composite

specific applications. At a microscopic level, properties of composites depend on the individual properties of the fiber and matrix as well as the orientation of the fiber in the matrix. The unidirectional fibers are the simplest arrangement of fibers in a fiber-reinforced composite and are shown in Fig. 2.10. In these composites, minimum properties are given along the transverse direction, whereas the maximum properties are given along the fiber-oriented direction.

Unidirectional Fiber–Matrix Composites Unidirectional composites possess different tensile moduli in various directions and are presented in Fig. 2.11a-b.

Longitudinal Tensile Modulus The following assumptions have been used for determining the longitudinal tensile modulus:

(i) Longitudinal load produces equal strain in fiber and matrix.
(ii) Fibers are uniform, parallel, and continuous.
(iii) Perfect bonding between fiber and matrix. The net load applied (F_l) on the oriented direction of the fibers is shared by fibers (F_f) and matrix (F_m), which can be written by Eq. 2.27.

$$F_l = F_f + F_m \tag{2.27}$$

The stresses depend on the cross-sectional area of fiber (A_f) and matrix (A_m). Then, Eq. 2.27 is written as Eq. 2.28.

$$\sigma_l A = \sigma_f A_f + \sigma_m A_m \tag{2.28}$$

where A, σ_f, and σ_m are the total cross-sectional area of the composite, the fiber stress, and the matrix stress, respectively. The total cross-sectional area of the composite is given by

$$A = A_f + A_m \tag{2.29}$$

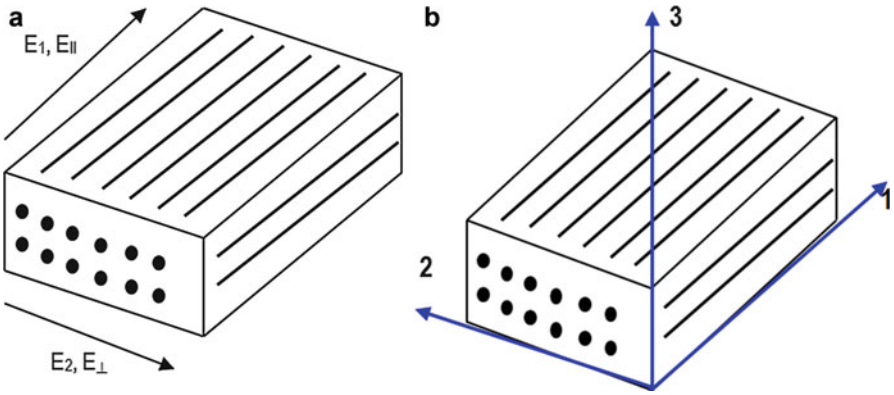

Fig. 2.11 Different tensile moduli labeled (**a**) in various ways and (**b**) in different directions

From Hooke's law, Eq. 2.28 is written as Eq. 2.30

$$E_1 \varepsilon_1 A = E_f \varepsilon_f A_f + E_m \varepsilon_m A_m \tag{2.30}$$

where E_1, E_f, E_m, ε_1, ε_m, and ε_f are the axial Young's modulus of the composite, the axial modulus of the fiber, the axial modulus of the matrix, the strain on the composite, the strain on the fiber, and the strain on the matrix, respectively.

However, the strain is same on the fibers (ε_f), the matrix (ε_m), and the composite (ε_1) and can be written as

$$\varepsilon_1 = \varepsilon_f = \varepsilon_m \tag{2.31}$$

Then the Eq. 2.30 is reduced to Eq. 2.32.

$$E_1 A = E_f A_f + E_m A_m \tag{2.32}$$

Dividing both sides by the area "A," then Eq. 2.32 changes to Eq. 2.33.

$$E_1 = E_f \frac{A_f}{A} + E_m \frac{A_m}{A} \tag{2.33}$$

For a unidirectional composite,

$$\frac{A_f}{A} = V_f \tag{2.34}$$

$$\frac{A_m}{A} = V_m \tag{2.35}$$

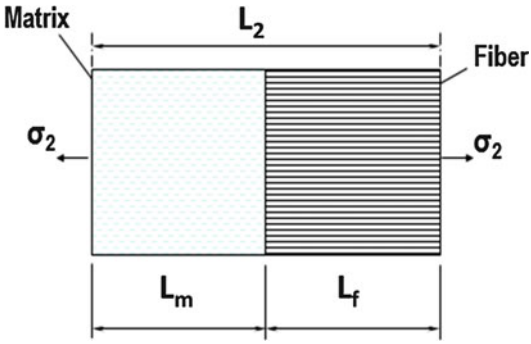

Fig. 2.12 Model showing transverse stiffness of a unidirectional composite

where V_f and V_m are the volume fraction of the fiber and volume fraction of the matrix, respectively. Then the tensile modulus of the composite in the longitudinal direction can be represented by Eq. 2.36 [78].

$$E_1 = E_f V_f + E_m V_m \tag{2.36}$$

For density, this is similar to the rule of mixtures. For polymer composites, $E_f >> E_m$. Therefore, $E_1 \approx E_f V_f$.

Transverse Tensile Modulus For predicting the transverse tensile property, plenty of mechanical models have been used. One of such a simple model is Jones model [79]. In this model, a load, which is applied in a direction normal to the fibers, contributes for the transverse stiffness. The fibers are stacked together and the model is being simplified. It is assumed that the stresses are equal in each of the components [i.e., composite stress in the transverse direction (σ_2) = fiber stress (σ_f) = matrix stress (σ_m)], and also the Poisson contraction effects are ignored. A model showing transverse stiffness of a unidirectional composite is depicted in Fig. 2.12.

The total extension (δ_2) = $\delta_f + \delta_m$. If the total elongation in the load direction is L_2, and the elongation on the fibers and matrix are L_f and L_m, respectively, then length and strains are written by Eqs. 2.37 and 2.38, respectively.

$$\varepsilon_2 L_2 = \varepsilon_f L_f + \varepsilon_m L_m \tag{2.37}$$

where ε_2, ε_f, and ε_m are the composite strain, fiber strain, and matrix strain, respectively.

Dividing Eq. 2.37 both sides by L_2, then

$$\varepsilon_2 = \varepsilon_f \frac{L_f}{L_2} + \varepsilon_m \frac{L_m}{L_2} \tag{2.38}$$

However, $L_f/L_2 = V_f$ and $L_m/L_2 = V_m = (1–V_f)$. Therefore, strain becomes (Eq. 2.39),

$$\varepsilon_2 = \varepsilon_f V_f + \varepsilon_m (1 - V_f) \tag{2.39}$$

where V_f and V_m are the volume fraction of the fiber and volume fraction of the matrix, respectively.

By using Hooke's law, Eq. 2.39 can be written as Eq. 2.40:

$$\frac{\sigma_2}{E_2} = \frac{\sigma_f V_f}{E_f} + \frac{\sigma_m (1 - V_f)}{E_m} \tag{2.40}$$

However, $\sigma_2 = \sigma_f = \sigma_m$; hence, Eq. 2.40 becomes Eq. 2.41 [79].

$$E_2 = \frac{E_m E_f}{E_m V_f + E_f (1 - V_f)} \tag{2.41}$$

where E_2, E_m, and E_f are the modulus of composite in the transverse direction, modulus of the matrix, and modulus of the fiber, respectively. It is observed that E_2 is not particularly sensitive to V_f. If $E_f >> E_m$, E_2 becomes independent of the property of the fiber. The matrix dominates the transverse modulus and is virtually independent of the reinforcement. Jones model is not relevant to most of the practical situations. Hence, improved mechanical models have been developed by using the theoretical studies such as Halpin–Tsai model [80]. The semiempirical Halpin–Tsai equations [81, 82] correct the Eq. 2.41 as

$$E_2 = \frac{E'_m E_f}{E'_m V_f + E_f (1 - V_f)} \tag{2.42}$$

where $E'_m = [E_m/(1 - \nu^2_m)]$ and ν_m is the Poisson's ratio of the matrix.

Hull et al. in 1996 have predicted the rule of mixtures for longitudinal (E_1) and transverse (E_2) modulus of glass/polyester composite ($E_f = 73.7$ MPa, $E_m = 4$GPa) as shown in Fig. 2.13 [83].

Stiffness of Short Fiber Composites For short fiber (aligned) composites, which are usually not found in polymers, the rule of mixtures for modulus [84] in the fiber direction is given as:

$$E_c = \eta_L E_f V_f + E_m (1 - V_f) \tag{2.43}$$

where E_c, η_L, E_f, E_m, and V_f are the modulus of the short fiber composite in the fiber direction, the length correction factor, the modulus of the fiber, the modulus of the matrix, and the volume fraction of the fiber, respectively. The length correction factor (η_L) is obtained theoretically (for $L > 1$ mm, $\eta_L > 0.9$).

The rule of mixture expression is brought into picture for composites in which fibers are not perfectly aligned by incorporating both η_L and η_o, where "η_o" is the correction for the non-unidirectional reinforcement. It is 1.0 for unidirectional,

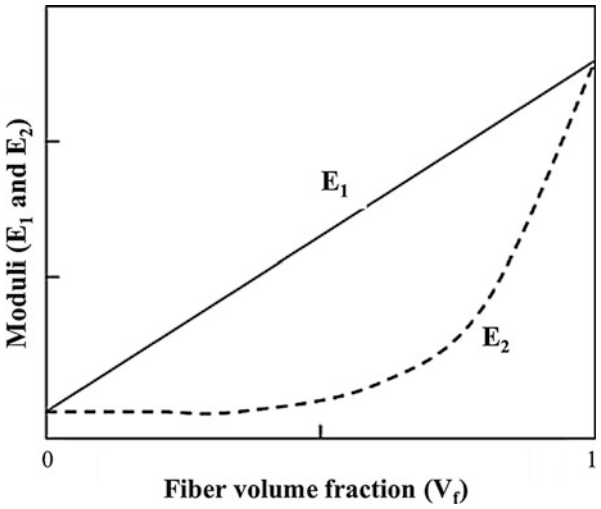

Fig. 2.13 Schematic showing rule of mixture prediction for longitudinal (E_1) and transverse (E_2) modulus [83]

0.5 for biaxial, 0.25 for biaxial at 45°, 0.375 for random in plane, and 0.2 for random in three dimensions.

In short fiber-reinforced thermoset polymer composites, the fibers are much longer than their critical length, and orientation effects determine the elastic properties. For the randomly oriented fiber, the following equations (Eqs. 2.44, 2.45, and 2.46) give sufficiently accurate estimates [85].

$$E_r = \frac{3}{8}E_{11} + \frac{5}{8}E_{22} \tag{2.44}$$

$$G_r = \frac{1}{8}E_{11} + \frac{1}{4}E_{22} \tag{2.45}$$

$$\nu_r = \frac{E_r}{2G_r} - 1 \tag{2.46}$$

where E_r, E_{11}, E_{22}, G_r, and ν_r are the modulus of randomly oriented fiber composite, longitudinal modulus of the composite, transverse modulus of the composite, shear modulus of the randomly oriented fiber composite, and Poisson's ratio of the randomly oriented fiber composite, respectively.

Fatigue

Fiber-reinforced composites have a good rating regarding fatigue life, which can be evaluated by S-N curve. Tension–tension fatigue of advanced composites can be tested with ASTM standard D-3479 specimen. Most of the composite materials are inhomogeneous and anisotropic, and the fatigue behavior of inhomogeneous

composites is much more complicated. A model proposed by Epparachchi et al. [86] is applicable to the fatigue data for glass/epoxy and glass/polypropylene specimens. The empirical fatigue law used is given below.

$$\frac{d\sigma}{dt} = -a\sigma_{max}(1-R)^{\gamma}t^{-k} \tag{2.47}$$

where σ, t, σ_{max}, R, and γ are the applied stress, time, maximum stress applied, stress ratio, and the set fixed to 1.6 (derived from assumption on fatigue crack propagation rate), respectively, and a and k are constants.

The above model can be arranged as follows [86]:

$$\left(\frac{\sigma_{ult}}{\sigma_{max}} - 1\right)\frac{1}{(1-R)^{\gamma}}f^{\beta} = \alpha\left(N^{\beta} - 1\right) \tag{2.48}$$

where σ_{ult}, σ_{max}, f, and N are the ultimate stress, the maximum stress applied, the loading frequency, and the number of loading and unloading cycles till failure, respectively, and α and β are constants (can be determined experimentally).

A model has also been developed for the fatigue testing of E-glass fiber/epoxy composite, and the model equations [87] are given as follows:

$$\frac{d\sigma}{dt} = -C_2 t^{-m_1} \tag{2.49}$$

$$C_2 = A.f(R, \sigma_u, \sigma_{max}) \tag{2.50}$$

where σ, t, m_1, A, R, σ_u, and σ_{max} are the residual strength after n cycles, time, a material constant, a constant, stress ratio, the initial residual strength, and the maximum applied stress, respectively.

Creep

Creep can be defined as high-temperature progressive deformation at constant stress. It is a performance-based behavior since it is not an intrinsic material response. It is highly dependent on environmental conditions such as temperature. A creep test involves a tensile specimen under a constant load maintained at a constant temperature, and strain measurements are recorded over a period of time. A standard method of testing the creep and creep rupture of a continuous fiber-reinforced ceramic composites subjected to tensile loading at elevated temperature is according to ASTM C-1337:96. The creep resistance of MgO/SiC nanocomposite is found to be 2–3 times greater than that of pure MgO matrix at a temperature of 1300 °C and for the Al_2O_3/SiC nanocomposite, it is about 3–4 times greater than that of a pure Al_2O_3 matrix at a temperature of 1400 °C. In these two cases, a tremendous improvement in creep resistance is observed. This is attributed to the suppression of grain boundary slidings by the reinforced intergranular nano-sized SiC particles.

Stress Relaxation

Glass fiber-reinforced polymer (GFRP) composites used for structural applications require good, long-term mechanical properties. This behavior can be predicted by accelerated mechanical testing such as creep and stress relaxation. The dimensional stability of load-bearing structures and the retention of clamping force for bolts fastened to composites are determined by stress relaxation behavior. The stress relaxation studies of pineapple leaf fiber-reinforced polyethylene composites and banana fiber-reinforced polyester composites have been studied [88, 89]. Barpanda and Mantena have studied the effects of hybridization on the stress relaxation and creep characteristics of pultruded glass–epoxy–graphite hybrid composites [90]. The dynamic mechanical analysis is used for the stimulated stress relaxation and creep testing. Geethamma et al. have analyzed the tensile stress relaxation of natural rubber composites reinforced with short-coir fiber [91]. The strain rate, fiber orientation, and loading affect the relaxation mechanisms of both filled and unfilled composite. Kawai et al. have studied stress relaxation of unidirectional T800H/3631 epoxy/carbon composite at comparatively high tensile strain levels and at elevated temperature [92]. This test has been carried out at 100 °C on plain coupon samples having different fiber orientations, $\theta = 0$, 10, 30, 45, and 90°. After maintaining the constant strain, relaxation of the axial stress with time takes place in a short period. In composite materials, the stress relaxation rate inclines to become zero, regardless of the orientation of the fiber. The relaxation modulus associated with stress relaxation depends on the strain level. The creep and stress relaxation studies to determine the time-dependent longitudinal strength of epoxy and polyester composites reinforced with unidirectional glass fiber have been reported by Lifshitz and Rotem [93]. The risk of delayed fracture can be avoided for stress values lower than 0.4 and 0.65 times the ultimate failure stress for the glass–polyester and glass–epoxy composites, respectively. Gutman and Soncino have analyzed the stress relaxation in polyester–fiber–glass composite under different temperature and chemical environments [94]. Wortmann and Schulz have studied the stress relaxation properties of polypropylene fibers at different temperatures (−50 to 30 °C) [95]. The moduli and relaxation time show noticeable temperature dependencies. Ikeda has assessed the chemical resistance of fiber-reinforced plastics using stress relaxation analysis [96].

Performance Under Adverse Conditions

Polymer matrix composites are sensitive to the changes in environmental conditions such as extreme temperatures, moisture, etc. The effects of temperature and moisture on the parameters such as tensile strength, ILFT, ILSS, elastic modulus, fatigue, etc. have to be examined for better understanding. Hashemi et al. have determined the influence of temperature and geometry on the mode-I, mode-II, and mixed mode-I/mode-II ILFT of the CF/PEEK composites [97]. The study is done within the temperature range 20–130 °C. An increase in ILFT with increase in temperature is

observed. However, the ILFT at sub-zero temperatures has not been determined. Sloan and Seymour have investigated the impact on mode-I interlaminar fracture and crack growth in graphite/epoxy as a result of exposing to seawater [98]. Takeda et al. have studied the ILFT of epoxy matrix CFRP and GFRP composites irradiated by high-energy electrons [99]. In case of GFRP, a significant decrease in the fracture toughness is noticed. The effect of moisture on the ILFT of particle-filled glass fiber-reinforced polyester resin composites has been investigated by Srivastava and Hogg [70]. The samples are exposed to water at 20 and 40 °C. Mode-I and mode-II ILFT are measured at an interval of 2 months. It is reported that mode-I toughness is increased for all composites with an increasing moisture uptake. Watt et al. have studied the changes to the mode-I ILFT of stitched fiberglass/vinyl ester composites after exposure to elevated temperatures between 100 and 300 °C [100]. The ILFT of the stitched composites degrades significantly by heating. Pavlidou and Papaspyrides have analyzed the effect of hygrothermal history on the ILSS of glass/polyester composites [101]. The experimentation is carried out at a temperature of 35 °C. Davies et al. have studied the effect of seawater aging on the shear behavior of glass-reinforced composites at 20 and 50 °C [102]. Apicella et al. have studied polyesters and their glass mat-reinforced composites at 20 °C and 90 °C for 50 days [103]. Choqueuse et al. have done a detailed research in a 2-year period on distilled water aging at temperatures 5, 20, 40, and 60 °C [104].

Thermal

Thermal characterization is very important to achieve precise measurement before the application. The thermal behavior of composite materials is evaluated based on the coefficient of thermal expansions (CTEs). Since CTEs vary from material to material, the thermal properties of the composite may be altered. The CTEs are given by Eqs. 2.51 and 2.52 [1].

$$\alpha_l = \frac{V_f \alpha_{fl} E_{fl} + V_m \alpha_m E_m}{V_f E_{fl} + V_m E_m} \tag{2.51}$$

$$\alpha_t = V_f \alpha_{ft} \left(1 + \nu_{flt} \frac{\alpha_{fl}}{\alpha_{ft}}\right) + V_m \alpha_m (1 + \nu_m) - (V_f \nu_{flt} + V_m \nu_m) \alpha_l \tag{2.52}$$

where α_l, α_t, α_{fl}, α_{ft}, E_{fl}, α_m, E_m, ν_{flt}, and ν_m are the coefficient of thermal expansion in the longitudinal direction, coefficient of thermal expansion in the transverse direction, coefficient of thermal expansion of fibers in the longitudinal direction, coefficient of thermal expansion of the fibers in the transverse direction, the modulus of fibers in the longitudinal direction, coefficient of thermal expansion of the matrix, the modulus of matrix, the in-plane Poisson's ratio of fibers, and Poisson's ratio of the matrix, respectively, and the other variables are as discussed above.

Similarly, the longitudinal (Eq. 2.53) and transverse (Eq. 2.54) thermal conductivities of the composite can be written [1] as

$$K_l = V_f K_{fl} + V_m K_m \tag{2.53}$$

$$K_t = \frac{K_{fl} K_m}{V_f K_m + V_m K_{ft}} \tag{2.54}$$

where K_l, K_{fl}, K_m, K_t, and K_{ft} are the thermal conductivity of the composite in the longitudinal direction, the thermal conductivity of fibers in the longitudinal direction, the thermal conductivity of the matrix, the thermal conductivity of the composite in the transverse direction, and the thermal conductivity of fibers in the transverse direction, respectively, and the other variables are as discussed above.

Ceramic matrix composites are the materials for high-temperature applications. Various composites have been prepared with SiC matrices, SiC fibers, and boron nitride (BN) fiber coatings [105]. High deposition temperature CVD is the most desirable technique for BN fiber coatings; however, it may lead to problems in the composite fabrication. In this composite, there appears to be three important mechanisms for BN oxidation corrosion: (i) borosilicate glass formation, (ii) gettering (is the process of removing device-degrading impurities from the active regions) of oxygen by SiC, and (iii) volatilization [105]. Rochais et al. have performed initial tests on known materials and a carbon–carbon composite with the help of different analysis methods [106]. These methods explain the modifications in the experimental setup as indicated in Fig. 2.14, a procedure used to determine the temperature diffusivity. The experimental setup has three main parts: (i) an optical setup for positioning and focusing the probe beams and the pump used, (ii) device used for measuring the intensity of the probe beam, and (iii) various electronic devices, which are used for detecting the signal and carrying out the experiment. Maximum power of the pump beam, which is a continuous Ar laser, is 2 W. Its frequency is modulated by a frequency generator-driven acousto-optic modulator operated at frequencies up to 2 MHz. Then, the pump beam is directed with the help of dichroic mirror, which is finally focused with the help of microscope onto the sample surface in the heating stage. The probe beam, which is a laser diode (wavelength 780 nm, power 20 mW), passes through a quarter-wave plate and the dichroic mirror, which is then focused with the same microscope on to the sample surface. After reflecting back, it retracts through the quarter-wave plate again, and from there it is sent to the photodiode by a beam splitter cube. A pump beam photon is protected from reaching the detector by using an optical filter. The amplitude and phase of the periodic signal collected by the photodiode is extracted by a lock-in amplifier. The dichroic mirror orientation is controlled by a PC controller, which governs the distance "r" between the probe and pump beam locations. Heating stage window, which is made of fused silica, transmits 93 % of the intensity of the two beams. Specifically designed objective (40 × magnification) with a large working distance, which is capable of correcting the spherical aberrations produced due to the heating stage window, has been used. Heating stage could attain a highest temperature of 1500 °C under a vacuum level better than 10^{-3}mbar. Sample polishing is necessary in order to ensure good

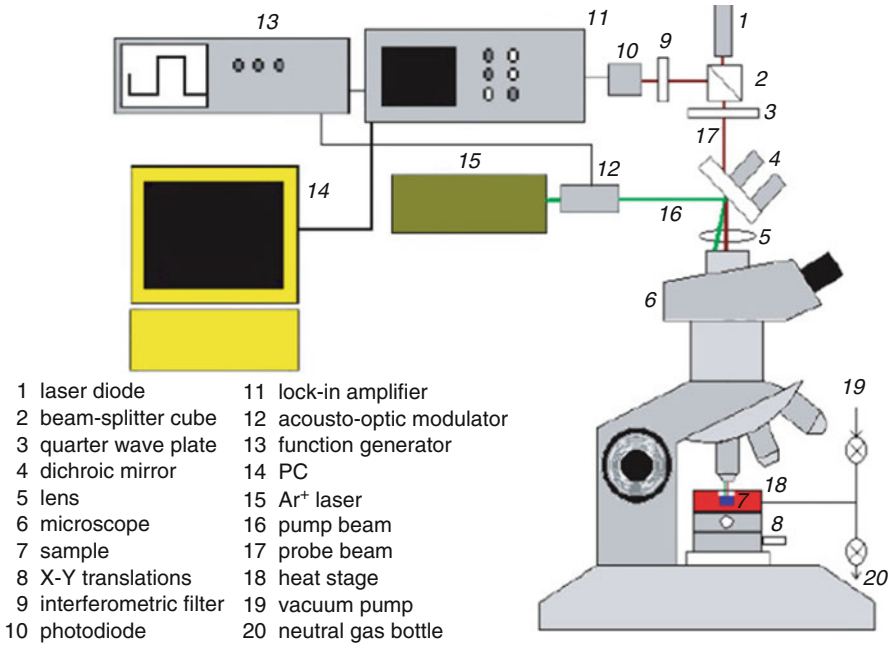

Fig. 2.14 Schematic of a thermal microscope setup [106]

reflection. The sample has a diameter less than 7 mm and thickness c.a. 1 mm. Homogeneous temperature gradient is maintained by keeping the thickness of sample as small as possible.

Glass Transition Temperature

Glass transition temperature (denoted by "Tg") is the temperature at which a material experiences a significant change in properties from hard and brittle to soft and pliable. Typically, Young's modulus changes sharply. At glass transition temperature, the polymeric structure turns "rubbery" upon heating and "glassy" upon cooling. The glass transition temperature of composites can be determined with the help of differential scanning calorimetry (DSC) technique. It is to be noted that in the case of low Tg materials, in order to achieve the benefit of orientation enhancement effect, the Tg should be in the vicinity of or lower than the measuring temperature.

Electrical

The uses of electrically conductive polymers (ECPs) have been limited in the past due to their drawbacks such as poor mechanical properties, poor environmental and thermal stabilities, etc. It has been shown that the composite structure using an

insulating polymer as the host matrix improves the physical and chemical properties of ECPs. These composites can have practical advantages over the homogeneous materials. In the high-temperature region, the electrical conductivity (σ) of the films is found to follow the equation given below [107]:

$$\sigma = \sigma_0 \exp\left(-\frac{E_a}{kT}\right) \tag{2.55}$$

where E_a, T, and k are the activation energy, absolute temperature, and Boltzmann constant, respectively. It has been reported that the mechanical properties of the conductive composites can be improved with a decrement in the electrical conductivity [107]. Lee and Chen have proposed an idea for improving the mechanical strength of conventional ceramic superconductors, where they have found applications in magnetic levitation and shielding [108]. A series of composites have been prepared, which are flexible even at high temperatures (e.g., $(Bi,Pb)_2Sr_2Ca_2Cu_3O_x$ (2223)). A low-melting-point thermoplastic polymer, nylon-6,6, is used as structural matrix for the composite preparation. The superconducting $(Bi,Pb)_2Sr_2Ca_2Cu_3O_x$, (2223) powder with critical temperature $T_c \sim 104$ K has been prepared by conventional solid state reactions having a nominal composition of $Bi_{1.6}Pb_{0.4}Sr_2Ca_2Cu_3O_y$ [108].

Magnetic

Magnetic materials in the field of micromachining have been an area of interest for applications such as electromagnetic interference shielding, integrated inductive components, and magnetic microactuators and sensors. However, those materials possessing desirable hard magnetic properties might not be compatible with that of the standard microelectronic processes. For example, in preparation of magnets demanding high temperature, sintering, and pressing, such as in neodymium–iron–boron and samarium–cobalt magnets [109]. Magnetic polymer composites are made of strontium ferrite powder embedded in the polyimide organic matrix. These are considered to be compatible with the micromachining and microelectronic processes and they exhibited good magnetic properties, such as a high coercivity (c.a. 320 kA/m), square magnetization curve, a residual induction approaching 0.3 T, and a maximum energy product of 11,900 T (A/m) and are comparable to the bulk ferrite [109]. Nanostructured magnetic materials exhibit properties stemming from the intrinsic character of the particles and interactions between the particles. These magnetic properties often differ from both the individual constituent atoms and bulk crystalline counterparts. For soft magnetic properties, exchange coupling between the magnetic nanocrystalline grains is required. Therefore, freestanding nanoparticles must be consolidated to allow for this exchange coupling. A ferromagnetic nanocomposite having magnetic nanocrystalline particles in the polymeric matrix can replace conventional ferrites for various applications such as chokes, high-frequency inductors, filters, sensors, core-shaped planar transformers, etc. The

increase in resistivity leads to a major reduction in the eddy-current losses in the magnetic/polymeric nanocomposite solid, while the coupling between adjacent magnetic nanoparticles produces remarkably better soft magnetic properties at larger frequencies compared with ferrites or conventional bulk materials.

Piezoelectric

Piezoelectric and electrostrictive materials are found applications in transducers and sensors. Their role in a sensing device is to detect displacement, acceleration, force, and sound. Hence, they are widely used in applications, such as strain and vibration measurement; medical, structural, and health monitoring; underwater imaging; etc. In the last two decades, the ceramics (e.g., lead titanate), polymers (e.g., polyvinylidene difluoride and its copolymers), and ceramic polymer composites (e.g., piezoelectric ceramic particles LaRC Si polyamide binder matrix composite) have been used as piezoelectric materials. Some of the electrostrictive materials have been found to produce a relatively high strain (e.g., lead magnesium niobate) with less hysteresis than that of piezoelectric materials. The piezoelectricity is commonly defined by the following equations [110]:

$$\varepsilon_i = S_{ij}^{E}\sigma_j + d_{mi}E_m \tag{2.56}$$

$$D_m = d_{mi}\sigma_i + \zeta_{ij}^{\sigma}E_k \tag{2.57}$$

where ε, S, σ, d, E, D, and ζ are the strain vector (in m/m), matrix of compliance coefficients (in m^2/N), stress vector (in N/m^2), matrix of piezoelectric strain constants (in m/V), vector of applied electric field (in V/m), vector of electric displacement (in C/m^2), and permittivity (in F/m), respectively. Here, i and j varies from 1 to 6, and m and k varies from 1 to 3. Also, the superscripts E and σ represent that the measurements are taken at constant electric field and constant stress, respectively.

In polycrystalline ceramics, the poled axis is usually denoted as the 3-axis, and with the ceramic having C_α symmetry, the number of nonzero matrix elements is 10 (like s_{11}^E, s_{12}^E, s_{13}^E, s_{33}^E, s_{44}^E, d_{31}, d_{33}, d_{15}, ε_{11}^T, and ε_{33}^T). Piezoelectric materials exhibit dispersion and the various material constants are function of frequencies. Most of the constants can be calculated by using resonance measurements. The resonance measurements are carried out by using small signals on the specimens. A test methodology has been developed to characterize the piezoelectric fiber composite for structural actuations as an alternative to monolithic piezoceramic wafers. By using interdigitated electrode pattern, the performance of the abovementioned actuator system has been improved, which helps in the orientation of the electric field's primary component in the plane of the structure, thus permitting the use of piezoelectric effect along the active fibers. This technology can be applied in an integral twist actuation of helicopter rotor blades for large harmonic control. The actuators

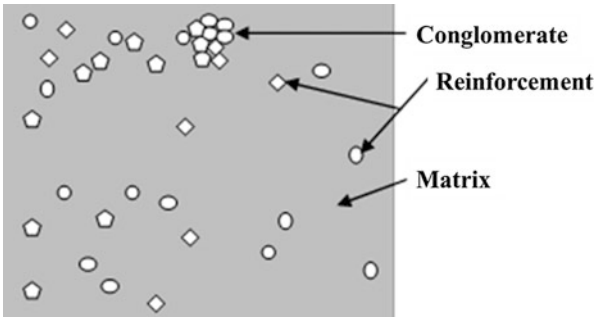

Fig. 2.15 Schematic of piezoelectric ceramic particles reinforced LaRC Si polyamide composite

required in this application must be able to counter the effect of harsh operating conditions for rotor blades of the helicopter. Thus, actuators that can withstand a huge number of electrical and mechanical cycles with appreciable centripetal and bending loads are desired. The performance of several actuators including S2 glass-reinforced and E-glass-laminated actuators have been studied. It has been observed that the abovementioned interdigitated electrode piezoelectric fiber composite actuator has a wide range of ability for the heavy loading requirements. The micromechanical piezoelectric composites consisting of LaRC Si polyamide binder and piezoelectric ceramic particles, to serve as sensors and actuators for space applications, have been developed. A schematic of this composite is shown in Fig. 2.15. In this schematic, piezoelectric ceramic particles (reinforcement) are indicated by lighter in color, and the darker region is an indicative of LaRC Si polyamide binder (matrix).

It has been shown that the ceramic particles are bound together in a conglomerate configuration. This typical feature plays a significant role to determine the thermomechanical response of the composite. It is known that a combination of negative coefficient of thermal expansion for ceramic phase and a positive coefficient of thermal expansion for LaRC Si phase results in a nonzero coefficient of thermal expansion for a piezoelectric composite. An application of thermal loading will result in internal stresses due to the thermomechanical and the piezoelectric response. The theoretical models have been developed for studying the piezoelectric behavior of lead titanate (up to 70 vol.%) and polyvinylidene difluoride composites. It has been observed that the data are matched with the experimental results. The piezoelectric polymer (PEP) composites have shown different piezoelectric relaxations. The dispersion has been prepared by adding 3–0 PEP composite piezoelectric spheres in a continuous polymer medium. When an electric field is applied to such a composite, each piezoelectric spheres experiences polarization and can be represented as a dipole. The dipole moment locally modifies the applied field and the surrounding medium. When only a small volume fraction of piezoelectric spheres are present, the influence of this dipole field on the neighboring field will be negligible.

Tribological

Tribological properties of composites are highly significant in long-term application point of views. The erosive wear behavior of Al_2O_3-fiber MMCs has been widely studied [111]. The erosion testing apparatus consists of a stainless steel T-tube in the slurry tank above an erodent reservoir, as shown in Fig. 2.16. The T-tube acts as a vacuum pump by circulation mechanism of water via. a loop arrangement, and the SiC particles (size ~ 600–800 μm) are driven up for impinging the slurry jet onto the specimen. The system gives a certain concentration (e.g., 5.6 wt%) of SiC particles, a jet velocity (e.g., 7.3 m/s) with a flow rate of water (e.g., 4.6 lit/min). The impact angle can be easily adjusted in this arrangement. The distance between the targets can be altered as per our requirements, and the ejector nozzle as well as their relative positions can be easily shuffled and can be monitored. The samples of dimension 25 mm × 25 mm × 5 mm are cut from an Al-MMC cast in two directions – one parallel to the fiber (Al-MMC-P) and the other vertical to the fiber (Al-MMC-V). An Al-alloy (K8510) matrix blank sample without fiber has been used. It has been observed that in the initial stages, the erosion rate (E) rises with the impact angle to

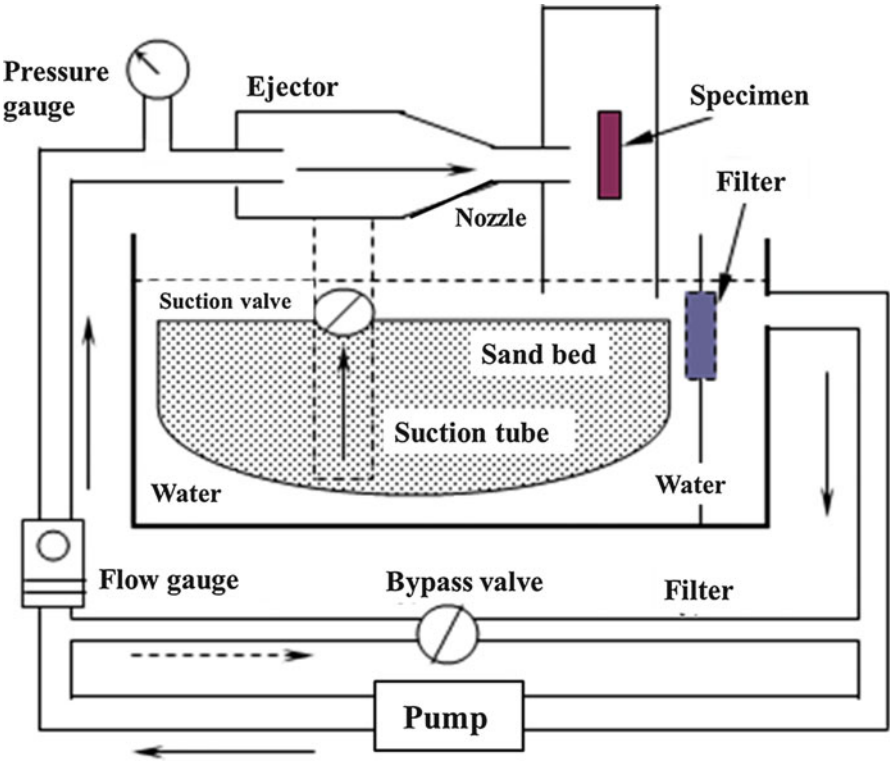

Fig. 2.16 Schematic of erosion test apparatus of sand/water slurry [111]

the maximum and decreased very lethargically then after, with further increase in the erosion angle (α).

Bearing Strength

For an aircraft, bearing strength greatly influences the composite component designs. When applied through a cylindrical fastener surface, the maximum stress that a composite can withstand is known as the bearing strength. The bearing stress is an applied comprehensive load on an interface divided by the bearing area. Bearing strength of composite materials can be tested with standard specimen ASTM.00008.10. Furthermore, bearing strength of advanced composite materials can be tested with standard specimen SACMA SRM 9–88. Due to high dependence of notch sensitivity on laminate configuration and a lower shear and bearing strength, having a satisfactory efficiency for a structural coupling with mechanical fastening is very difficult for the composite materials when compared with metals. These properties actually restrict the structural performance of the composite structure and require special reinforcement techniques. Fink and Kolesnikov have observed a high bearing strength for CFRP/Ti hybrid composites while performing bearing tests with specimens having different Ti content unidirectional prepreg plies [112]. In this study, carbon specimens with different laminate configurations have also been tested for comparison. A 6 mm diameter bolt is used and has given a clearance fit with the clamping torque of 0–0.6 mm. The tested specimens featured an edge distance to diameter ratio of 3 and a width to diameter ratio of 4 and 5. The characteristics of static tests conducted up to the failure in on-axis and 90°-off-axis loading directions are illustrated in Fig. 2.17.

Here, the maximum specific on-axis bearing strength of the hybrid material is noticed at a Ti content of 55 %, which is slightly lower in comparison to that of 50/40/10 carbon laminate, while 90°-off-axis bearing strength is about 40 % higher.

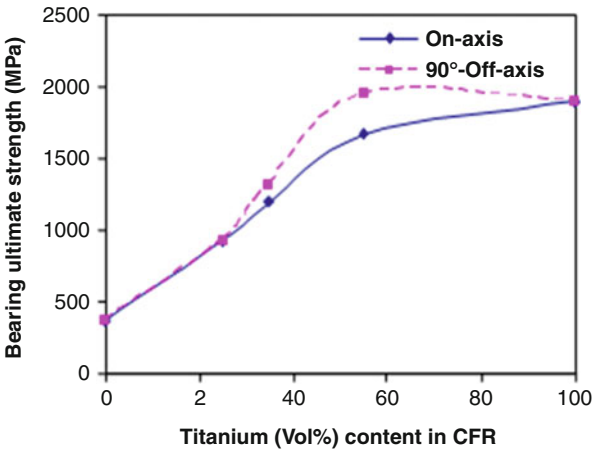

Fig. 2.17 Dependency of bearing strength of a hybrid material on Ti content [112]

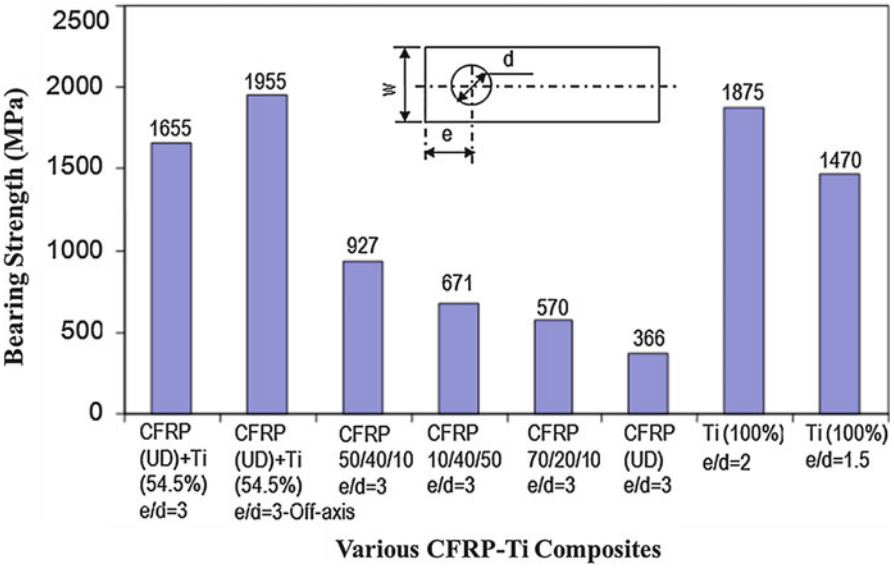

Fig. 2.18 Bearing strength of various CFRP-Ti composites [112]

However, the laminate-specific strength doesn't reflect the absolute weight efficiency of the joint, since the laminate represents only a fraction of the whole local joint design of the structure. The realization of high absolute joint strengths contributes to the reduced complexity and weight of secondary joint components such as bolts, fittings, and connecting parts to a high extent, thus reducing the overall joint weight. The test results have shown the advantage of Ti-reinforced composite material, which offers an increase in strength about 80 % under on-axis loading and 180 % under 90°-off-axis loading compared to the bearing properties of a 50/40/10 CF laminate and is shown in Fig. 2.18. Higher strength increase rates result when comparing with laminates having a higher degree of anisotropy. Hybrid material containing 54 % Ti offers a bearing strength similar to that of a Ti-alloy.

A bearing test apparatus for an aerospace grade unidirectional CF prepreg tape is shown in Fig. 2.19. The materials such as standard moduli CFs and 180 °C cure modified, toughened epoxy resin have been used for the bearing test experiment [113]. In this experiment, the fasteners with free running nut, 6.35 mm diameter steel hex head bolts, and plain steel washers having 12.7 mm diameter are used. The experimental matrix is comprised of six coupons with the following local constraint conditions: (i) a torque of 0.6, 1.3, 2.4, 3.5, or 7.0 Nm is given to the fastener and (ii) 0.5 or 0.1 mm gap is given on each side of the composite coupon. A mode of failure has been observed and is concluded that the level of local constraints (applied torque or gap size) affects the bearing strength. The gap values between 0.5 and 1.0 mm do not influence the initial failure load. Although, if failure is initiated, debris filling the gap will increase that leads the bearing strength values that do not actually shows the pin-bearing behavior. For an increase in torque values above 1.3 Nm,

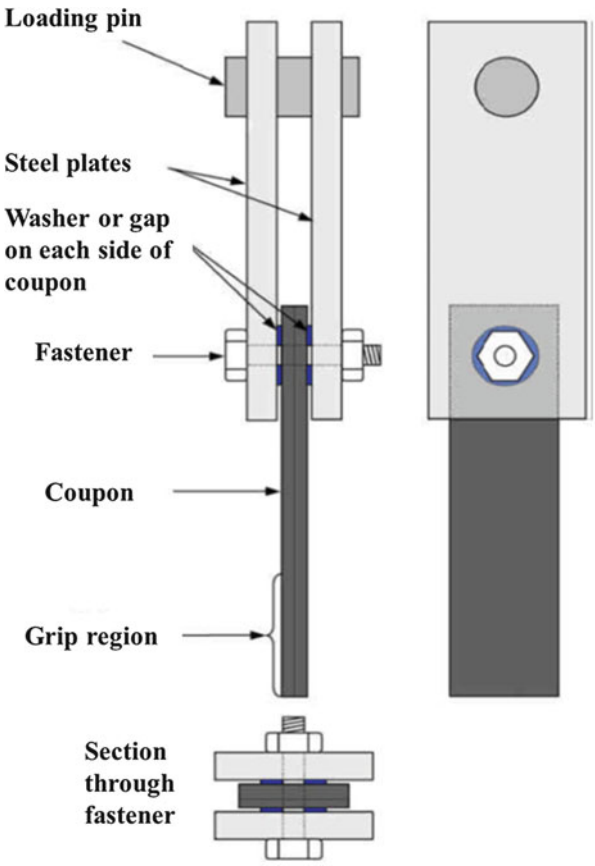

Fig. 2.19 Bearing test apparatus for aerospace grade unidirectional carbon fiber prepreg tape [113]

there is a slight increase in bearing strength, which is steady in nature, and with the increase in values of torque between 0 and 1.3 Nm, the bearing strength increases rapidly. A typical bearing stress–strain for each constraint condition is shown in Fig. 2.20.

Rheological

Rheology is the study of the flow of liquids but also solids under conditions in which they flow rather than deform elastically. It is applicable to substances, which have a complex structure, including muds, sludges, suspensions, polymers, many foods, bodily fluids, biological materials, and composites. The rheological performance of long fiber-reinforced thermoplastic composite has been developed, and its relation to structural aspects, which stem from different processing routes used, and correlation of observed facts with available theories have been focused by Cervenka and Alan [114]. The materials for the study are selected in such a way that the role of all

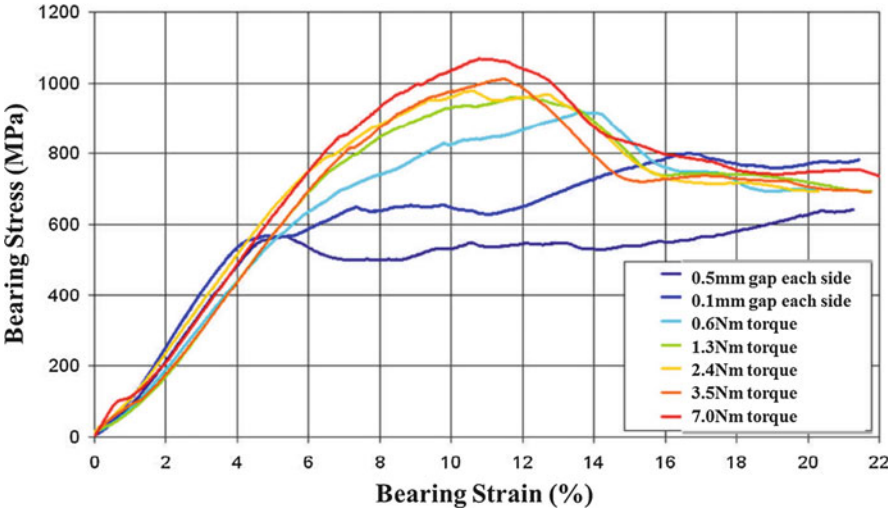

Fig. 2.20 A typical bearing stress–strain for each constraint condition [113]

important variables known to control the composite performance can be assessed. The important variables are as follows:

1. The type of matrix: polypropylene and polyamide
2. The nature of the fiber: glass, carbon, and Kevlar
3. Processing methods: classical injection molding and multiple life-feed techniques
4. Initial fiber length: 5 and 10 mm long pellets used as the feedstock for both the processing methods.

In this study, measurements of rheological parameters and quantification of relevant structural features together with generation of data for composites have been conducted simultaneously. The different structures of thermoplastic matrix/fiber constituents of different mechanical properties are related to the rheological behavior of heterogeneous melts and the interfacial behavior between the matrix and the reinforcement. Shi et al. have studied the rheological properties with good amount of dispersion of single-walled nanotubes (SWNTs) at low concentrations (0.05 wt%) in uncross-linked poly(propylene fumarate) [115]. It has been observed that the SWNTs aggregate at higher concentrations. This aggregation ratifying the mechanical and rheological properties has been revealed with the help of scanning electron microscopic study of fractured nanocomposite surfaces. The oscillatory shear viscoelastic (dynamic and linear) response for an uncross-linked nanocomposite and an uncross-linked polymer with varying concentrations of SWNTs, which are made compatible with the polymer using 12-aminododecanoic acid surfactant, is shown in Fig. 2.21 [115]. The complex viscosity magnitude ($|\eta^*|$) and the elastic modulus (G') both transforms abruptly from liquid-like behavior of the matrix polymer ($G' \propto \omega^2$, $|\eta^*| \propto \omega^0$) to solid-like behavior of the nanocomposites having 0.05 wt% and higher SWNT ($G' \propto \omega^0$, $|\eta^*| \propto \omega^{-1}$).

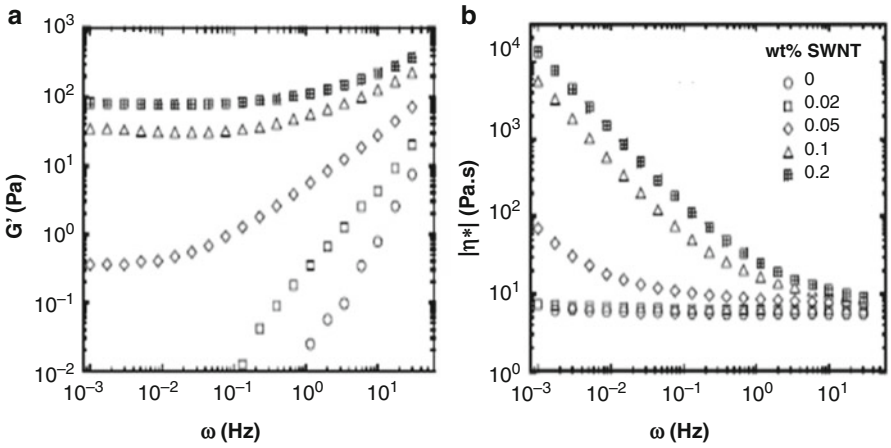

Fig. 2.21 Schematic showing dependency of (**a**) elastic modulus and (**b**) complex viscosity magnitude on frequency [115]

Biological

Biological characterizations of composite materials include toxicity and degradation testing procedures, which are most important in biological applications [116–119]. The interphases of such composites are particularly important in the case of bio-related applications; hence, their properties in terms of biocompatibility, biodegradability, and bioactivity have to be well understood before practical applications [120, 121]. For example, the dental patients have routinely demanded high aesthetic restorations since a long time ago. The major problems related to the use of resin composites for large restorations in posterior teeth are the side effects and environmental issues related with dental amalgams. The current developments in dental researches have evoked the interest on the use of ceramic composite materials for restoration application [122]. Research on novel biodegradable, biocompatible, and bioactive composite materials for various biological applications such as bone replacement [123–127], tissue replacements [128–132], etc., are on the way to success.

Concluding Remarks

In this chapter, the various experimental characterizations of composites are discussed briefly. Since these characterizations are not adequate for determining complete properties of the composite systems, advanced techniques have to be developed in order to obtain a broad picture. The need of highly performing advanced composites is increasing day by day due to the developments on their processability, designing flexibility, etc. The advanced composites are often

presenting greatest challenges in their experimental characterizations. Among these, biological characterization is also very important since the toxicity of composites will directly influence the human life. Hence, characterizing composite materials for the better understanding of their real behaviors, in all possible directions, is very critical for their practical applicability and acceptance.

Acknowledgment The authors acknowledge the financial support provided by the Indian Space Research Organization, India, for carrying out this work.

References

1. Astrom BT (2002) Manufacturing of polymer composites. Nelson Thornes, Cheltenham
2. Ravi S, Iyengar NGR, Kishore NN, Shukla A (2000) Influence of fiber volume fraction on dynamic damage in woven glass fabric composites: an experimental study. Adv Compos Mater 9:319
3. Gdoutos EE, Pilakoutas K, Rodopoulos CA (2000) Failure analysis of industrial composite materials. McGraw-Hill, New York
4. Kelly A (1990) Concise encyclopedia of composite materials. MIT Press, Cambridge
5. ASTM D 3171–06 (2006) Standard test methods for constituent content of composite materials. Annual Book of ASTM Standards 15.03
6. ASTM D 2584–02 (2006) Standard test method for ignition loss of cured reinforced resins. Annual Book of ASTM Standards 8.01
7. Wu Y, Shivpuri R, Lee LJ (1998) Effect of macro and micro voids on elastic properties of polymer composites. J Reinf Plast Compos 17:1391
8. Summerscales J (1987) Non-destructive testing of fibre-reinforced plastics composites. Elsevier Science Publishers, London
9. Bowles KJ, Frimpong S (1992) Void effects on the interlaminar shear strength of unidirectional graphite fiber-reinforced composites. J Compos Mater 26:1487
10. Chambers AR, Earl JS, Squires CA, Suhot MA (2006) The effect of voids on the flexural fatigue performance of unidirectional carbon fibre composites developed for wind turbine applications. Int J Fatigue 28:1389
11. ASTM D 1505–03 (2006) Standard test method for density of plastics by the density-gradient technique. Annual Book of ASTM Standards 8.01
12. ASTM D 3800–99 (2006) Standard test method for density of high-modulus fibres. Annual book of ASTM standards 15.03
13. Zahavi E, Torbilo V (1996) Fatigue design: life expectancy of machine parts. CRC Press, Boca Raton
14. Graham TS (2002) Industrial metrology: surfaces and roughness. Springer, Berlin
15. Davim JP, Reis P (2005) Damage and dimensional precision on milling carbon fiber-reinforced plastics using design experiments. J Mater Process Technol 160:160
16. Savage G (1993) Carbon-carbon composites. Chapman and Hall, London
17. Kessler MR (2004) Advanced topics in characterization of composites. Trafford Publishing, Victoria
18. Theocaris PS, Stassinakis CA (1981) Crack propagation in fibrous composite materials studied by SEM. J Compos Mater 15:133
19. Kreider KG (ed) (1974) Metallic matrix composites. Academic, London
20. Hill RG (1968) Evaluation of elastic moduli of bilaminate filament-wound composites – crazed and uncrazed coupons from a rocket case and laboratory panel are subjected to static and dynamic loading. Exp Mech 8:75
21. Lantz RB (1969) Boron epoxy laminate test method. J Compos Mater 3:642

22. Richards GL, Airhart TP, Ashton JE (1969) Off-axis tensile coupon testing. J Compos Mater 3:586
23. Pagano NJ, Halpin JC (1968) Influence of end constraint in the testing of anisotropic bodies. J Compos Mater 2:18
24. ASTM D 3039 (2006) Standard test method for tensile properties of polymer matrix composite materials. Annual Book of ASTM Standards 15.03
25. Niihara K et al (1996) High temperature strength and creep behavior of ceramic based nanocomposites roles of intergranular nano-sized particulates. In: Hui D (ed) Proceedings of the 3rd international conference on composite engineering (ICCE/3), New Orleans, 1996
26. Daniel IM, Gdoutos EE, Rajapakse YDS (eds) (2009) Major accomplishments in composite materials and sandwich structures. Springer, London
27. Thomas S, Joseph K, Malhotra SK, Goda K, Sreekala MS (eds) (2012) Polymer composites, volume 1, macro- and microcomposites. Wiley-VCH, Weinheim
28. Hsu PW, Herakovich CT (1977) Edge effects in angle-ply composite laminates. J Compos Mater 11:422
29. Pipes RB, Pagano NJ (1970) Interlaminar stresses in composite laminates under uniform axial extension. J Compos Mater 4:538
30. Wang JTS, Dickson JN (1978) Interlaminar stress in symmetric composite laminates. J Compos Mater 12:390
31. Gu Y, Liang G (2006) Self-reinforced interlayer shearing intensity resin base fibre reinforced composite material preparation method. Chinese Patent 1,762,686
32. Sato H, Suzuki Y (2005) Polyacrylonitrile-based carbon fibre and method for producing the same. JP Patent 2,005,314,830
33. Barelko VV et al (2005) Fibre-glass reinforcing weave filler for polymeric glass composites. RU Patent 2,245,477
34. Goto K et al (2004) Epoxy resin composition prepreg and fibre-reinforced composite material. JP Patent 2,004,292,594
35. Muraki T, Nishiyama S (2003) Method for producing high-density fibrous structure and the resultant high-density fibrous structure. JP Patent 2,003,073,968
36. Mortaigne B, Regnier N (2000) Study of epoxy and epoxy–cyanate networks thermal degradation to predict materials lifetime in use conditions. J Appl Polym Sci 77:3142
37. Wu SJ, Lin TK, Zhang JX, Shyu SS (2000) Properties of cyanate ester-cured epoxy/polyphenylene oxide blends as a matrix material for Kevlar fiber composites. J Adhes Sci Technol 14:1423
38. Ratna D, Chongdar TK, Chakraborty BC (2004) Mechanical characterization of new glass fiber reinforced epoxy composites. Polym Compos 25:165
39. DeCarli M, Kozielski K, Tian W, Varley R (2005) Toughening of a carbon fibre reinforced epoxy anhydride composite using an epoxy terminated hyperbranched modifier. Compos Sci Technol 65:2156
40. Matheswaran M, Padmanabhan K, Kishore (1995) Static and impact behavior of thermoplastic modified glass fabric/epoxy composites. J Mater Sci Lett 14:951
41. Sainathan N, Padmanabhan K, Sashidhara S, Rao RMVGK, Kishore (1995) Influence of particulate graphite additions on the shear related behavior of glass fabric reinforced epoxy composites. J Reinf Plast Compos 14:445
42. Podgaiz RH, Williams RJJ (1997) Effects of fiber coatings on mechanical properties of unidirectional glass-reinforced composites. Compos Sci Technol 57:1071
43. John NA, Brown JR (1998) Flexural and interlaminar shear properties of glass-reinforced phenolic composites. Compos Part A 29A:939
44. Cho D, Yun SH, Kim J, Lim S, Park M, Lee S-S, Lee G-W (2004) Influence of silane coupling agents on the interlaminar and thermal properties of woven glass fabric/nylon 6 composites. Macromol Res 12:119
45. Barraza HJ, Aktas L, Hamidi YK, Long J Jr, Orear EA, Altan MC (2003) Moisture absorption and wet-adhesion properties of resin transfer molded (RTM) composites containing elastomer-coated glass fibers. J Adhes Sci Technol 17:217

46. Park R, Jang J (2004) Effect of surface treatment on the mechanical properties of glass fiber/vinylester composites. J Appl Polym Sci 91:3730
47. Li Y, Mai Y-W, Ye L (2005) Effects of fibre surface treatment on fracture-mechanical properties of sisal-fibre composites. Compos Interfaces 12:141
48. Zhang C, Hoa SV, Ganesan R (2002) Experimental characterization of interlaminar shear strengths of graphite/epoxy laminated composites. J Compos Mater 36:1615
49. Okada T, Nishijima S (1990) Investigation of interlaminar shear behavior of organic composites at low temperatures. Adv Cryog Eng 36B:811
50. Vishwanath B, Verma AP, Rao CVSK (1991) Effect of fabric geometry on friction and wear of glass fiber-reinforced composites. Wear 145:315
51. Costa ML, Almeida SFMD, Rezende MC (2005) Critical void content for polymer composite laminates. AIAA J 43:1336
52. Ray BC (2006) Loading rate sensitivity of glass fiber-epoxy composite at ambient and sub-ambient temperatures. J Reinf Plast Compos 25:329
53. Ray BC (2006) Loading rate effects on mechanical properties of polymer composites at ultralow temperatures. J Appl Polym Sci 100:2289
54. Mouritz AP (2000) Ultrasonic and interlaminar properties of highly porous composites. J Compos Mater 34:218
55. Smith JC, Blandford JM, Schiefer HF (1960) Stress–strain relationships. In yarns subjected to rapid impact loading. Text Res J 30:752
56. Chocron-Benloulo IS, Sanchez-Galvez V (1996) Impact resistance of polymeric matrix composites. In: Hui D (ed) Proceedings of the third international conference on composite engineering (ICCE/3), New Orleans, 1996
57. Mueller DH (2004) Improving the impact strength of natural fiber reinforced composites by specifically designed material and process parameters. INJ Winter 31:28
58. Foster GC (1998) Tensile and flexure strength of unidirectional fiber reinforced composites: direct numerical simulations and analytic models. Dissertation, Virginia Polytechnic Institute and State University
59. Dash PK, Chatterjee AK (2004) Effects of environment on fracture toughness of woven carbon/epoxy composite. J Inst Eng 85:1
60. Kim J-K, Mai Y-W (1993) Interfaces in composites. In: Chou TW (ed) Structure and properties of fibre composites, vol 13. VCH Publishers, Weinheim, pp 239–289
61. Metcalfe AG (ed) (1974) Interfaces in metal matrix composites. Academic, London
62. Wilkins DJ, Eisenmann JR, Camin RA, Margolis WS, Benson RA (1982) Characterizing delamination growth in graphite-epoxy. In: Reifsnider KL (ed) Damage in composite materials. ASTM International, Philadelphia, p 168
63. Han KS, Koutsky J (1981) The interlaminar fracture energy of glass fiber reinforced polyester composites. J Compos Mater 15:371
64. Devitt DF, Schapery RA, Bradley WL (1980) A method for determining the mode I delamination fracture toughness of elastic and viscoelastic composite materials. J Compos Mater 14:270
65. Mall S, Law GE, Katouzian M (1987) Loading rate effect on interlaminar fracture toughness of a thermoplastic composite. J Compos Mater 21:569
66. Feih S, Wei J, Kingshott P, Sorensen BF (2005) The influence of fibre sizing on the strength and fracture toughness of glass fibre composites. Compos Part A Appl S 36:245
67. Tanoglu M, Seyhan AT (2003) Investigating the effects of a polyester preforming binder on the mechanical and ballistic performance of E-glass fiber reinforced polyester composites. Int J Adhes Adhes 23:1
68. Compston P, Jar P-YB, Davies P (1998) Matrix effect on the static and dynamic interlaminar fracture toughness of glass-fiber marine composites. Compos Part B Eng 29:505
69. Kuboki T, Jar PYB, Forest TW (2003) Influence of interlaminar fracture toughness on impact resistance of glass fiber reinforced polymers. Compos Sci Technol 63:943

70. Srivastava VK, Hogg PJ (1998) Moisture effects on the toughness, mode-I and mode-II of particles filled quasi-isotropic glass-fiber reinforced polyester resin composites. J Mater Res 33:1129
71. Kang TJ, Lee SH (1997) Mechanical properties of nonwoven glass fiber composites. Polym Polym Compos 5:29
72. Shetty MR, Kumar KRV, Sudhir S, Raghu P, Madhuranath AD, Rao RMVGK (2000) Effect of fiber orientation on mode-I interlaminar fracture toughness of glass epoxy composites. J Reinf Plast Compos 19:606
73. Sela N, Ishai O, Banks-Sills L (1989) The effect of adhesive thickness on interlaminar fracture toughness of interleaved CFRP specimens. Composites 20:257
74. Yang Z, Sun CT (2000) Interlaminar fracture toughness of a graphite/epoxy multidirectional composite. J Eng Mater Technol 122:428
75. Yuan Q, Karger-Kocsis J (1996) On the efficiency of interleaves in carbon fiber/epoxy composite laminates by the fractal approach. J Mater Sci Lett 15:842
76. Barikani M, Saidpour H, Sezen M (2002) Mode-I interlaminar fracture toughness in unidirectional carbon-fiber/epoxy composites. Iran Polym J 11:413
77. Shindo Y, Shinohe D, Kumagai S, Horiguchi K (2005) Analysis and testing of mixed-mode interlaminar fracture behavior of glass-cloth/epoxy laminates at cryogenic temperatures. J Eng Mater Technol 127:468
78. Stinchcomb WW, Ashbaugh NE (eds) (1993) Composite materials fatigue and fracture. ASTM International, Philadelphia
79. Wang R-M, Zheng S-R, Zheng Y (2011) Polymer matrix composites and technology. Woodhead Publishing, Cambridge
80. Halpin Affdl JC, Kardos JL (1976) The Halpin-Tsai equations: a review. Polym Eng Sci 16:344
81. Halpin JC, Tsai SW (1967) Environmental factors in composite design. In: Airforce materials laboratory technical report, AFML-TR-67-423
82. Clyne TW, Withers PJ (1993) An introduction to metal matrix composites. Cambridge University Press, Cambridge
83. Hull D, Clyne TW (1996) An introduction to composite materials. Cambridge University Press, Cambridge
84. Lu L, Fuh J (2001) Laser-induced materials and processes for rapid prototyping. Kluwer Academic Publishers, Boston
85. Campbell FC (2010) Structural composite materials. ASM International, Materials Park
86. Epparachchi JA, Clausen PD (2000) A new approach to a fatigue damage model for glass-fiber reinforced plastic composites. In: Hui D (ed) Proceedings of the seventh international conference on composites engineering, ICCE/7, Denver 2000
87. Toumi RB, Renard J, Monin M, Nimdum P (2013) Fatigue damage modelling of continuous E-glass fibre/epoxy composite. Procedia Eng 66:723
88. Sreekala MS, Kumaran MG, Joseph R, Thomas S (2001) Stress-relaxation behaviour in composites based on short oil-palm fibres and phenol formaldehyde resin. Compos Sci Technol 61:1175
89. Pothan LA, Neelakantan NR, Rao B, Thomas S (2004) Stress relaxation behavior of banana fiber-reinforced polyester composites. J Reinf Plast Compos 23:153
90. Barpanda D, Mantena PR (1998) Effect of hybridization on the creep and stress relaxation characteristics of pultruded composites. J Reinf Plast Compos 17:234
91. Geethamma VG, Pothen LA, Rhao B, Neelakantan NR, Thomas S (2004) Tensile stress relaxation of short-coir-fiber-reinforced natural rubber composites. J Appl Polym Sci 94:96
92. Kawai M, Kazama T, Masuko Y, Tsuda H, Takahashi J, Kemmochi K (2004) Stress relaxation behavior of unidirectional carbon/epoxy composites at elevated temperature and analysis using visco-plasticity mode. JSME Int J A-Solid M 47:8

93. Lifshitz JM, Rotem A (1970) Time-dependent longitudinal strength of unidirectional fibrous composites. Fibre Sci Technol 3:1
94. Gutman EM, Soncino R (1995) Environmental effect on stress relaxation in polyester-fiberglass composite. Polym Compos 16:518
95. Wortmann F-J, Schulz KV (1995) Stress relaxation and time/temperature superposition of polypropylene fibers. Polymer 36:315
96. Ikeda S (1987) Evaluation of the chemical resistance of fiber-reinforced plastics by stress relaxation method. Nippon Zairyo Gakkai 26:127
97. Hashemi S, Kinloch AJ, Williams JG (1990) The effects of geometry, rate and temperature on the mode I, mode II and mixed-mode I/II interlaminar fracture of carbon fiber/poly(ether ether ketone) composites. J Compos Mater 24:918
98. Sloan FE, Seymour RJ (1992) The effect of seawater exposure on Mode I interlaminar fracture and crack growth in graphite/epoxy. J Compos Mater 26:2655
99. Takeda N, Tohdoh M, Takahashi K (1995) Interlaminar fracture toughness degradation of radiation-damaged GFRP and CFRP composites. Adv Compos Mater 4:343
100. Watt A, Goodwin AA, Mouritz AP (1998) Thermal degradation of the Mode I interlaminar fracture properties of stitched glass fiber/vinyl ester composites. J Mater Sci 33:2629
101. Pavlidou S, Papaspyrides CD (2003) The effect of hygrothermal history on water sorption and interlaminar shear strength of glass/polyester composites with different interfacial strength. Compos Part A 34:1117
102. Davies P, Mazeas F, Casari P (2001) Sea water aging of glass reinforced composites: shear behaviour and damage modelling. J Compos Mater 35:1343
103. Apicella A, Migliaresi C, Nicolais L, Iaccarino L, Roccotelli S (1983) The water ageing of unsaturated polyester-based composites: influence of resin chemical structure. Composites 14:387
104. Choqueuse D, Davies P, Mazeas F, Baizeau R (1997) Aging of composites in water: comparison of five materials in terms of absorption kinetics and evolution of mechanical properties. In: Gates TS, Zureick A-H (eds) High temperature and environmental effects on polymeric composites, vol 2. ASTM International, Philadelphia, p 73
105. Jacobson NS, Fox DS, Opila EJ (1998) High temperature oxidation of ceramic matrix composites. Pure Appl Chem 70:493
106. Rochais D, Houedec HL, Enguehard F, Jumel J, Lepoutre F (2005) Microscale thermal characterization at temperatures up to 1000°C by photoreflectance microscopy: application to the characterization of carbon fibers. J Phys D Appl Phys 38:1498
107. Kiralp S, Kucukyavuz Z, Qasrawi AF (2003) Preparation and characterization of conducting polybutadiene/polythiophene composites. Turk J Chem 27:417
108. Lee SL, Chen TM (1993) Preparation and characterization of a ceramic superconductor/nylon 6,6 composite. Chin J Phys 31:1175
109. Lagorce LK, Allen MG (1997) Magnetic and mechanical properties of micromachined strontium ferrite/polyimide composites. J Microelectromech Syst 6:307
110. Moheimani SOR, Fleming AJ (2006) Piezoelectric transducers for vibration control and damping. Springer, London
111. Fang Q et al (1996) Erosive wear behaviour of Al_2O_3-fiber reinforced aluminium based metal matrix composites (MMCs). In: Hui D (ed) Proceedings of the third international conference on composite engineering, ICCE/3, New Orleans, 1996
112. Fink A, Kolesnikov B (2005) Hybrid titanium composite material improving composite structure coupling. Accessed 09 July 2015. http://www.dlr.de/fa/Portaldata/17/Resources/dokumente/publikationen/2005/08_fink.pdf
113. Ferguson R (2004) Effect of local constraint on measured bearing stress in carbon/epoxy laminate. In: Proceedings of the 2nd international conference on composites testing and model identification, Bristol, 21–23 Sept 2004
114. Cervenka A, Allan PS (1997) Characterization of finite length fiber composites: Part I. Introductory paper (technical report). Pure Appl Chem 69:1693

115. Shi X, Hudson JL, Spicer PP, Tour JM, Krishnamoorti R, Mikos AG (2005) Rheological behavior and mechanical characterization of injectable poly(propylenefumarate)/single-walled carbon nanotube composites for bone tissue engineering. Nanotechnology 16:S531
116. Fung YC (1993) Biomechanics: mechanical properties of living tissues. Springer, New York
117. Wang M, Porter D, Bonfield W (1994) Processing, characterisation, and evaluation of hydroxyapatite reinforced polyethylene composites. Br Ceram Trans 93:91
118. Wang M, Bonfield W (2001) Chemically coupled hydroxyapatitepolyethylene composites: structure and properties. Biomaterials 22:1311
119. Wang M, Kokubo T, Bonfield W (1996) A-W glass–ceramic reinforced polyethylene composite for medical applications. Bioceramics 9:387
120. Wang M, Bonfield W, Li M, Guiu F (1996) Interphase in composite materials. Key Eng Mater 127:583
121. Guild FJ, Bonfield W (1993) Predictive modeling of hydroxyapatitepolyethylene composite. Biomaterials 14:985
122. Bergman MA (1999) The clinical performance of ceramic inlays: a review. Aust Dent J 44:157
123. Bonfield W (1987) Materials for the replacement of osteoarthritic hip joints. Met Mater 3:712
124. Kikuchi M, Itoh S, Ichinose S, Shinomiya K, Tanaka J (2001) Self-organization mechanism in a bone-like hydroxyapatite/collagen nanocomposites synthesized in vitro and its biological reaction in vivo. Biomaterials 22:1705
125. Reis RL, Cunha AM, Fernandes MH, Correia RN (1997) Bioinert and biodegradable polymeric matrix composites filled with bioactive SiO_2-3CaO.P_2O_5-MgO glasses and glass–ceramics. In: Bioceramics Vol.10. Elsevier Science, pp 415–418 Paris, France
126. Sousa RA, Reis RL, Cunha AM, Bevis MJ (2000) Structure and properties of hydroxylapatite reinforced starch bone-analogue composites. Key Eng Mater 192–195:669
127. Ladizesky NH, Pirhonen EM, Appleyard DB, Ward IM, Bonfield W (1998) Fibre reinforcement of ceramic/polymer composites for a major load-bearing bone substitute material. Compos Sci Technol 58:419
128. Wang M (2003) Developing bioactive composite materials for tissue replacement. Biomaterials 24:2133
129. Wang M, Bonfield W, Hench LL (1995) Bioglass/high density polyethylene composite as a new soft tissue bonding material. In: Wilson J, Hench LL, Greenspan D (eds) Bioceramics 10. Elsevier Science, Oxford
130. Wang M, Yue CY, Chua B, Kan LC (1999) Hydroxyapatite reinforced polysulfone as a new biomaterial for tissue replacement. Bioceramics 12:401
131. Wang M, Yue CY, Chua B (2001) Production and evaluation of hydroxyapatite reinforced polysulfone for tissue replacement. J Mater Sci Mater Med 12:821
132. Wang M, Chua B (2002) Fatigue performance of a bioactive composite developed for hard tissue replacement. Bioceramics 15:935